HHS Public Access

Author manuscript

Neuron. Author manuscript; available in PMC 2024 October 04.

Published in final edited form as:

Neuron. 2023 October 04; 111(19): 3084–3101.e5. doi:10.1016/j.neuron.2023.09.009.

An inhibitory circuit-based enhancer of DYRK1A function reverses *Dyrk1a*-associated impairment in social recognition

Yu-Tzu Shih[1,2,3,4], **Jason Bondoc Alipio**[1,2,3,4], **Amar Sahay**[1,2,3,4]

[1]Center for Regenerative Medicine, Massachusetts General Hospital, Boston

[2]Harvard Stem Cell Institute, Cambridge

[3]Department of Psychiatry, Massachusetts General Hospital, Harvard Medical School, Boston

[4]BROAD Institute of Harvard and MIT, Cambridge, United States

SUMMARY

Heterozygous mutations in the Dual specificity tyrosine-phosphorylation-regulated kinase 1a *Dyrk1a* gene define a syndromic form of Autism Spectrum Disorder. The synaptic and circuit mechanisms mediating DYRK1A functions in social cognition are unclear. Here, we identify a social experience-sensitive mechanism in hippocampal mossy fiber-parvalbumin interneuron (PV IN) synapses by which DYRK1A recruits feed-forward inhibition of CA3 and CA2 to promote social recognition. We employ genetic epistasis logic to identify a cytoskeletal protein, ABLIM3, as a synaptic substrate of DYRK1A. We demonstrate that *Ablim3* downregulation in dentate granule cells of adult heterozygous *Dyrk1a* mice is sufficient to restore PV IN mediated inhibition of CA3 and CA2 and social recognition. Acute chemogenetic activation of PV INs in CA3/CA2 of adult heterozygous *Dyrk1a* mice also rescued social recognition. Together, these findings illustrate how targeting DYRK1A synaptic and circuit substrates as “enhancers of DYRK1A function” harbors potential to reverse *Dyrk1a* haploinsufficiency-associated circuit and cognition impairments.

Graphical Abstract

Correspondence: asahay@mgh.harvard.edu.
Lead contact: asahay@mgh.harvard.edu

AUTHOR CONTRIBUTIONS

Conceptualization, AS; Methodology, JBA, YS, AS; Formal Analysis, JBA and YS; Investigation, JBA and YS; Resources, JBA, YS and AS; Writing, JBA, YS and AS; Visualization, JBA, YS and AS; Funding acquisition, AS

DECLARATION OF INTERESTS

A.S is a named inventor on US Patent 10, 287, 580 (Methods for inhibition of Ablim3 to improve memory in aging, Alzheimer’s disease and PTSD).

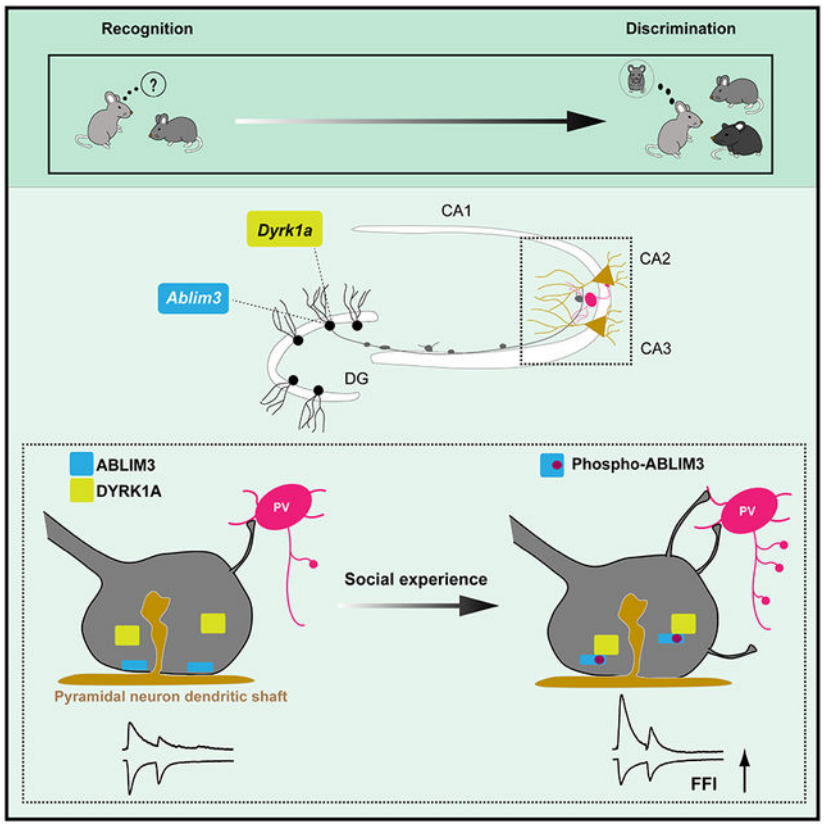

eTOC

Shih et al identify a synaptic and circuit mechanism by which DYRK1A regulates GABAergic inhibition and contributes to social recognition. Downregulation of a DYRK1A substrate, ABLIM3, in hippocampal mossy fiber-parvalbumin inhibitory neuron synapses in adulthood is sufficient to rescue *Dyrk1a* haploinsufficiency-associated impairments in parvalbumin inhibitory neuron functions and social recognition.

Keywords

dentate gyrus; *Dyrk1a* ; *Ablim3* ; Parvalbumin interneuron; social cognition; feed-forward inhibition; CA2; CA3; Hippocampus; epistasis; autism spectrum disorder

INTRODUCTION

Autism spectrum disorder (ASD) is a class of heterogeneous neurodevelopmental disorders that affects 1 in 100 children around the world and is characterized by impaired social cognition, repetitive behaviors, and increased seizure risk [1]. A fundamental challenge in identifying new treatments for ASD is understanding how disease gene mutations, grounded in robust human genetic signals, affect cellular, synaptic and circuit mechanisms underlying behavior [2]. Human genetic studies and large-scale exome-sequencing efforts implicate haploinsufficient loss-of-function (LOF) mutations in the Dual specificity tyrosine-phosphorylation-regulated kinase 1a *Dyrk1a* gene in syndromic ASD [3-5]. However,

the synaptic and circuit mechanisms by which DYRK1A affects social cognition are poorly understood. Currently, there are no drugs that enhance or restore DYRK1A function. This challenge is magnified because *Dyrk1a* is ubiquitously expressed in the developing and mature brain and DYRK1A phosphorylates more than 30 substrates that regulate diverse processes such as cell-cycle, neuronal migration, axonal and dendritic development, synapse formation, synaptic signaling and function [6-19]

One approach to developing strategies to restore DYRK1A function is to assess the potential for targeting DYRK1A synaptic substrates in social cognition circuits to reverse circuit- and social cognition impairments associated with *Dyrk1a* heterozygosity. Genetic epistasis guided logic [20,21] posits that potentiation of a downstream effector (i.e. synaptic substrate) of DYRK1A function should rescue DYRK1A dependent synaptic impairments and associated neural-circuit functions. Furthermore, although *Dyrk1a* haploinsufficiency associated impairments in social cognition arise from reduced DYRK1A mediated signaling and recruitment of different substrates throughout development, it is plausible that a subset of synaptic substrates may be targeted in adulthood to alleviate cognitive impairments.

Dentate gyrus (DG)-CA3/CA2 circuits play a critical role in encoding social experiences by integrating sensory information from association cortices, entorhinal cortex, prefrontal cortex and subcortical sites [22-43]. Prior work has shown that experience or learning increases dentate granule cell (DGC) recruitment of parvalbumin inhibitory neurons (PV IN) mediated perisomatic inhibition of CA3 neurons [44]. Anatomically, this manifests as an increase in number of mossy fiber terminal (MFT) filopodial contacts with PV INs and increase in number of PV IN perisomatic contacts (synapses on the cell bodies of excitatory pyramidal neurons that control excitatory pyramidal neuron output) in CA3 [44-49]. PV mediated perisomatic inhibitory synaptic transmission in downstream principal neurons (CA3/CA2) may facilitate encoding, routing and consolidation of experiential information in distinct neuronal ensembles by imposing a sparse activity regimen [50-53], synchronizing activity of principal cells, and generation of network oscillations [54-63]. Consistently, we recently demonstrated that increasing feed-forward inhibition (FFI) in DG-CA3 (i.e. DGC recruitment of PV IN mediated inhibition of CA3 neurons) resulted in enhanced stability and precision of context-associated neuronal ensembles and hippocampal-cortical synchrony [49]. Whether DGC recruitment of PV IN mediated inhibition of CA3 and CA2 is necessary for encoding social experiences is not known.

Studies using non-neuronal cells have shown that DYRK1A phosphorylates and functionally inactivates a family of F-actin stabilizing cytoskeletal proteins, ABLIMs, that results in destabilization of branched F-actin [64-66]. Extensive functional studies on ABLIMs 1-3 suggest that these highly homologous proteins mediate nucleation and bundling of linear and branched actin filaments to stabilize local cellular cortical actin networks essential for lamellipodia in leading edge of migrating cells [67-70]. Thus, ABLIM3 downregulation is predicted to destabilize branched F-actin, enhance actin disassembly and promote actin remodeling to generate filopodia, much like another class of cytoskeletal regulators in growth cones, MICALs, [71]. These studies were interesting to us as we had discovered that ABLIM3 in the hippocampus is restricted to mossy fiber terminals and that *Ablim3* downregulation in DGCs results in an increase in glutamatergic MFT-

filopodial contacts with PV INs, a process that we think depends on destabilization of branched F-actin in MFTs [44](https://hipposeq.janelia.org/full/t1/F64339A8-AF50-11E7-AD92-C0A401797C37/)[72]. Based on these observations, we hypothesized that DYRK1A phosphorylation of ABLIM3 in mossy fibers promotes DGC recruitment of PV IN mediated GABAergic inhibition in CA3 and CA2 to support social cognition. Furthermore, using functional genetic epistasis logic, we reasoned that if ABLIM3 functions downstream of DYRK1A in mossy fiber terminals (MFTs), then targeting *Ablim3* in DGCs may rescue *Dyrk1a* LOF associated impairments in social cognition.

Here, we show that social experience increases MFT-filopodial contacts with PV INs and PV IN perisomatic contacts in CA3 and CA2 pyramidal neurons. We demonstrate that *Dyrk1a* is necessary in DGCs of adult mice for feed-forward inhibition connectivity (MFT-filopodial contacts with PV INs), PV IN perisomatic contacts in CA3/CA2 and social recognition. We also demonstrate that ABLIM3 functions downstream of DYRK1A and is epistatic to DYRK1A in mossy fiber terminals. Based on these data, we use heterozygous *Dyrk1a* mice to show that loss of one *Dyrk1a* allele throughout development resulted in reduced MFT-filopodial contacts with PV INs, PV IN intrinsic excitability, PV IN perisomatic contacts in CA3/CA2 neurons and impaired social recognition in adulthood. These anatomical alterations were mirrored by reduced mossy fiber excitatory drive onto PV INs in CA3 and CA2 and mossy fiber recruitment of GABAergic inhibition of CA3 and CA2. Viral downregulation of *Ablim3* in DGCs of adult heterozygous *Dyrk1a* mice reversed these developmental anatomical and electrophysiological deficits and restored social recognition. Motivated by these findings, we assessed the impact of selectively activating PV INs in CA3/CA2 of adult heterozygous *Dyrk1a* mice on social recognition. We found that acute chemogenetic activation of PV INs in CA3/CA2 was sufficient to rescue social recognition impairments. Together, these findings illuminate how targeting DYRK1A synaptic substrates as “circuit-based enhancers of DYRK1A function” may harbor potential to reverse *Dyrk1a* haploinsufficiency-associated circuit and cognition impairments.

RESULTS

Dyrk1a is required in DGCs of adult mice for FFI connectivity, PV IN perisomatic contacts and social recognition

Learning increases mossy fiber excitatory drive onto PV INs [44,46-49] and enhances PV IN perisomatic contacts (“PV IN plasticity”) in CA3 [44,49]. To determine if social experience also increases FFI connectivity and PV IN plasticity in CA3/CA2, lentiviruses expressing GFP (CaMKIIα-GFP) were injected into the DG of 2-months old C57BL/6J mice two weeks prior to habituation to a context over 7 days. On day 8, mice were exposed to either the same context (context) or a novel juvenile mouse (social stimulus, same sex and strain) on day 8 (Figure 1A). 1.5 hours following social or context exposure we analyzed vGLUT1+ (vesicular glutamate transporter 1) mossy fiber terminal (MFT) filopodial contacts with PV INs and PV IN contacts (puncta) in CA3 and CA2 by immunohistochemistry. CA2 was labelled using the marker RGS14 (Regulator of G-protein signaling 14). Social experience increased MFT-filopodial contacts with PV INs and PV IN perisomatic contacts or “PV IN puncta density” in CA3 and CA2 (Figures 1B-1C).

We next asked whether *Dyrk1a* is necessary in DGCs for FFI connectivity and PV IN perisomatic contacts in CA3. *Dyrk1a* is expressed in all principal cell-types of the hippocampus (https://hipposeq.janelia.org). Immunostaining using antibodies that we validated for this study shows DYRK1A localization in MFTs (Figure 1D, Figure S1A). We injected lentiviruses expressing Cre-GFP under the control of CaMKIIα promoter into DG of adult *Dyrk1a*$^{+/+,\ f/+\ or\ f/f}$ mice [10,11] to delete one or both alleles of *Dyrk1a* in DGCs. Loss of one or both *Dyrk1a* alleles in DGCs (referred to as *Dyrk1a*$^{DGC\ f/+\ or\ f/f}$) did not change dendritic spine densities (Figures S1B-S1C) but decreased the number of VGLUT1+ MFT-filopodial contacts with PV INs and PV puncta (perisomatic synaptic contacts) density in CA3 (Figure 1E). Thus, normal gene dosage of *Dyrk1a* is necessary in DGCs for maintaining FFI connectivity and PV IN perisomatic contacts in CA3.

To determine if *Dyrk1a* is required in DGCs for social cognition, we tested adult wild-type mice (*Dyrk1a*$^{DGC+/+}$) or littermates in which *Dyrk1a* was virally deleted just in DGCs (*Dyrk1a*$^{DGC\ f/f}$) in a behavioral paradigm in which trial 1 (T1) probes encoding of a social stimulus or early stages of social recognition (often referred to as sociability), second and third trials (T2, T3) allow for familiarization to social stimulus and trial 4 (T4) tests discrimination of novel and familiarized social stimuli. In behavioral testing performed 2 weeks following lentiviral-Cre injections, we found that *Dyrk1a*$^{DGC\ f/f}$ mice did not exhibit a preference for the social stimulus over an empty cup indicating impaired social recognition (Figures 1F-1H, Figure S9A, **blue**). However, following familiarization trials T2 and T3, both groups of mice exhibited a comparable ability to distinguish a novel social stimulus from the familiarized social stimulus (Figures 1F-1H, Figure S9A, **yellow**). This suggests that extended exposure to social stimulus enables mice overcome deficiency in encoding of a social stimulus or early stages of social recognition. Supporting the notion that multiple trials of familiarization are necessary for *Dyrk1a*$^{DGC\ f/f}$ mice to successfully encode a social stimulus or for social recognition, we found that a single exposure of *Dyrk1a*$^{DGC\ f/f}$ mice to a social stimulus was insufficient to support successful discrimination of social stimuli (Figure S1D-S1E). Together, these data demonstrate that *Dyrk1a* is necessary in DGCs of adult mice for social recognition.

Analysis of *Dyrk1a*$^{DGC\ f/f}$ mice in assays for anxiety-like behavior, object preference, and novel object recognition suggested that deletion of *Dyrk1a* in DGCs of adult mice does not affect behavioral measures and performance in these domains (Figures S1F-S1J).

ABLIM3 functions downstream of DYRK1A in mossy fibers to regulate FFI connectivity, PV IN perisomatic contacts and social recognition

We had previously shown that ABLIM3 localizes to puncta adherens junctions in MFTs (visualized by immunostaining for zonula occludens 1, ZO1)-sites of stabilization of the MFT on dendritic shafts of CA3/CA2 neurons (Figure 1D) [44,73]. Since experience or viral mediated downregulation of *Ablim3* results in generation of MFT-filopodial contacts with PV INs [44,49] and DYRK1A phosphorylation of substrates may result in their degradation [11,64-66], we asked whether experience-dependent downregulation of ABLIM3 in mossy fiber terminals is dependent on DYRK1A. Towards this goal, we first generated heterozygous *Dyrk1a* mice (*EIIaCre; Dyrk1a* $^{f/+}$ or *Dyrk1a* $^{+/-}$) by breeding female *EIIa-Cre* mice with

male *Dyrk1a* $^{f/+}$ mice [11,74] *EIIa-Cre* mice carry a transgene under the control of the adenovirus EIIa promoter that targets expression of Cre recombinase to the preimplantation mouse embryo and are useful for germ line deletion of conditional alleles (JAX, Strain 003724) [75-77]. Analysis of EIIa-Cre activity using a Cre-reporter allele (Ai14, B6;129S6-*Gt(ROSA)26Sor*$^{tm14(CAG-tdTomato)Hze}$/J)[78] revealed widespread recombination in the brain (Figures S2A-S2B). Quantitative reverse transcription polymerase chain reaction (qRT-PCR) analysis of relative *Dyrk1a* expression in *EIIaCre; Dyrk1a* $^{f/+}$ mice showed an approximately fifty percent reduction in DG, CA2/CA3, sensorimotor cortex, and hypothalamus (Figure S2C). Next, we quantified ABLIM3 levels in MFTs in *Dyrk1a* $^{+/+ \text{ and } +/-}$ mice following a social experience (Figure 2A). We found that ABLIM3 levels in MFTs of heterozygous *Dyrk1a* mice did not decrease following social experience (Figure 2B-2C). Since levels of *Ablim3* transcripts were comparable in DG of *Dyrk1a* $^{+/+ \text{ and } +/-}$ mice (Figure S2D), these observations suggest that post-translational regulation of ABLIM3 is disrupted in *Dyrk1a* $^{+/-}$ mice.

The DYRK1A phosphorylation site in ABLIM3 is conserved across mammals [79-81] (Figure 2D) and across ABLIM family members (ABLIM1: SGRNSP, ABLIM2 SGRSTP, ABLIM3 SGRSSP). If ABLIM3 functions downstream of DYRK1A in the same pathway, then viral overexpression of an ABLIM3 phosphomimetic mutant that mimics DYRK1A phosphorylation of serine residue in ABLIM3 in DGCs will increase FFI connectivity and PV IN perisomatic contacts in CA3 in novel social experience naïve wild-type mice (homecage) i.e. result in a gain-of-function phenotype. Conversely, viral overexpression of an ABLIM3 loss-of-function phospho-dead mutant that has the serine residue in the DYRK1A phosphorylation site converted to an alanine residue, S->A) in DGCs should abrogate social experience-dependent increase in FFI connectivity and PV IN perisomatic contacts in CA3. Viral overexpression of an ABLIM3 phosphomimetic construct encoding ABLIM3 with a serine to aspartic acid amino acid substitution resulted in a significant increase in VGLUT1+ MFT filopodial contacts with PV INs and PV IN perisomatic contacts in CA3 (Figures 2E-2F) without affecting DGC dendritic spine densities (Figure S3A). Viral overexpression of the ABLIM3 phospho-dead mutant in DGCs abolished social experience-dependent enhancement of FFI connectivity and PV perisomatic contacts without affecting DGC dendritic spine densities (Figures S3A-S3C). Importantly, viral overexpression of ABLIM3 phospho-dead mutant in DGCs impaired social recognition (Figures S3A, S3D-S3E). As expected, none of these parameters were changed in home cage mice i.e novel social experience naïve mice expressing the ABLIM3 phospho-dead construct (Figures 2E-2F).

Our functional epistasis analysis positions ABLIM3 downstream of DYRK1A in mossy fiber terminals in social experience-dependent regulation of FFI connectivity and perisomatic contacts in CA3/CA2 (**working model,** Figure 2G). Based on these findings, we tested whether viral downregulation of *Ablim3* in DGCs is sufficient to rescue inhibitory circuitry impairments associated with *Dyrk1a* LOF in DGCs in adult mice. Viral injection of a construct co-expressing Cre and GFP under the ubiquitin *(Ubi)* promoter and an extensively previously validated shRNA targeting *Ablim3* in the same DGCs of adult *Dyrk1a* $^{+/+, f/+ \text{ or } f/f}$ mice [44,49](Figure S4A) rescued *Dyrk1a* loss of function-dependent reductions in VGLUT1+

MFT filopodial contacts with PV INs and PV IN puncta in CA3 (Figures 2H-2J) without affecting DGC dendritic spine densities (Figure S4B). These data support our model in which ABLIM3 functions downstream of DYRK1A in regulation of MFT-filopodial contacts with PV INs and PV IN plasticity (PV IN perisomatic contacts in CA3/CA2) (Figure 2G).

We next assessed whether viral *Ablim3* downregulation in DGCs also prevents the social recognition impairment seen following loss of *Dyrk1a* in DGCs. Behavioral analysis of adult mice expressing non-target shRNA (shNT) or *Ablim3* shRNA (shRNA) in DGCs in which one or both *Dyrk1a* alleles were deleted showed that viral downregulation of *Ablim3* reversed the social recognition impairment (Figure 2K, Figure S9B). We did not observe any effect of loss of one or both *Dyrk1a* alleles in DGCs or viral *Ablim3* downregulation in DGCs on locomotion in the open field, anxiety-like behavior, object preference or novel object recognition (Figures S4C-S4F).

Taken together, these findings demonstrate that loss of one allele of *Dyrk1a* in DGCs results in haploinsufficiency, reduced FFI connectivity, PV IN perisomatic contacts in CA3 and impaired social recognition. Additionally, ABLIM3 functions downstream of DYRK1A in DGCs of adult mice to mediate social recognition. These acute, cell-type restricted manipulations of *Dyrk1a* and *Ablim3* motivated us to ask whether mice lacking one allele of *Dyrk1a* throughout development (heterozygous *Dyrk1a* mice) show impairments in FFI connectivity, PV IN perisomatic contacts in both CA3 and in CA2 and social recognition in adulthood.

Ablim3 downregulation in DGCs of adult heterozygous *Dyrk1a* mice restores FFI connectivity and PV IN perisomatic contacts in CA3 and CA2

We injected lentiviruses expressing *Ablim3* shRNA-GFP or shNT-GFP into the DG of adult *Dyrk1a*$^{+/-}$ or $^{+/+}$ mice and analyzed dendritic spine densities of DGCs, DG-PV IN-CA3/CA2 connectivity and perforant path-DGC synapses (Figure 3A). DGCs of adult *Dyrk1a* $^{+/-}$ mice (shNT group comparisons) exhibited comparable dendritic spine densities compared to DGCs of *Dyrk1a* $^{+/+}$ mice (Figure S5A) but had significantly fewer VGLUT1+ MFT filopodial contacts with PV INs and PV IN perisomatic contacts in CA3 (Figures 3B-3C). We noted a trend towards a significant decrease in PV IN perisomatic contacts in CA2 subregion (Figure 3D). Lentiviral downregulation of *Ablim3* in DGCs of adult *Dyrk1a* $^{+/-}$ mice reversed these reductions in VGLUT1+ MFT filopodial contacts with PV INs and PV IN perisomatic contacts in CA3 and in CA2 without affecting dendritic spine densities (Figures 3B-3D).

Whole-cell recordings from DGCs of adult *Dyrk1a* $^{+/-}$ mice did not detect a difference in frequency or amplitude of miniature excitatory postsynaptic currents (mEPSCs) (Figure S5B, Supplementary Table 1). Analysis of electrically evoked EPSCs and inhibitory postsynaptic currents (IPSCs) from DGCs revealed comparable excitation-inhibition ratios and paired-pulse ratios (PPR) for *Dyrk1a* $^{+/+}$ and *Dyrk1a* $^{+/-}$ mice (Figure S5C). Viral downregulation of *Ablim3* in DGCs did not affect any of these measures. These observations suggest that DYRK1A or ABLIM3 do not functionally contribute to perforant path-DGC synapses (Figure S5C).

Together, these findings demonstrate that viral manipulation of *Ablim3* in DGCs of adult heterozygous *Dyrk1a* mice is sufficient to reverse developmental alterations in FFI connectivity and PV perisomatic contacts in both CA3 and in CA2. We next asked whether these anatomical changes in FFI and PV IN connectivity in DG-CA3/CA2 are mirrored by electrophysiological changes in feed-forward inhibition and GABAergic inhibition of CA3 and CA2 neurons.

Ablim3 downregulation in DGCs of adult heterozygous *Dyrk1a* mice restores inhibitory synaptic transmission in DG-CA2

To perform *ex vivo* whole-cell recordings from PV INs in *Dyrk1a*$^{+/-\text{ or }+/+}$ mice, we used a viral expression system, rAAV-S5E2-tdTomato, in which tdTomato expression is under the control of the "E2 regulator element" of the *Scn1a* gene (referred to as S5E2). S5E2 confers PV IN restricted expression (>90% specificity) in cortex and hippocampal CA1 of rodents [82]. To establish utility of using this viral expression system to selectively label PV INs in CA3/CA2, we analyzed the overlap of tdTomato and PV expression following viral injections into CA3/CA2. Systematic quantification in molecular and pyramidal layers of CA3 and CA2 revealed >90% overlap between tdTomato and PV expression (Figure S6A).

Next, we injected lentiviruses expressing *Ablim3* shRNA-GFP or shNT-GFP into DGCs and rAAV-S5E2-tdTomato into CA3/CA2 of adult (2-3 months) *Dyrk1a* $^{+/-\text{ or }+/+}$ mice and performed *ex vivo* whole-cell patch-clamp recordings from CA2 PV INs and CA2 pyramidal neurons (PNs) (Figure 4A, Supplementary Table 1). Consistent with reduced VGLUT1+ MFT filopodial contacts with PV INs in *Dyrk1a* $^{+/-}$ mice, we observed a significant reduction in frequency, but not amplitude, of miniature excitatory postsynaptic currents (mEPSCs) in PV INs (Figure 4B). In CA2 pyramidal neurons, we observed a reduction in frequency, but not amplitude, of miniature inhibitory postsynaptic currents (mIPSCs)(Figure 4C). We did not detect differences in frequency or amplitude of mEPSCs in CA2 pyramidal neurons in *Dyrk1a*$^{+/-}$ mice (Figure S6B). Viral downregulation of *Ablim3* in DGCs of *Dyrk1a* $^{+/-}$ mice completely reversed decrements in frequency of mEPSCs in PV INs in CA2 and frequency of mIPSCs in CA2 pyramidal neurons (Figures 4B-4C).

Next, we asked whether these developmental reductions in mossy fiber excitatory inputs onto PV INs and inhibitory inputs onto CA2 neurons in *Dyrk1a* $^{+/-}$ mice result in reduced DGC recruitment of FFI onto CA2. We virally expressed Channelrhodopsin (ChR2)[83] and shNT/shRNA in DGCs of *Dyrk1a* $^{+/+\text{ or }+/-}$ mice and recorded optically evoked excitatory and inhibitory post synaptic responses (oEPSCs and oIPSCs) in CA2 neurons following optogenetic stimulation of mossy fibers. *Dyrk1a* $^{+/-}$ mice exhibited a significantly higher ratio of oEPSCs and oIPSCs in CA2 pyramidal neurons compared to *Dyrk1a* $^{+/+}$ mice. This increase in the excitation-inhibition ratio was driven by a significant increase in oEPSCs and a reduction in oIPSCs in CA2 pyramidal neurons. Viral expression of *Ablim3* shRNA in DGCs of *Dyrk1a* $^{+/-}$ mice resulted in complete restoration of the excitation-inhibition ratio through a robust increase in oIPSCs and reduction in oEPSCs in CA2 pyramidal neurons. Bath application of DCG-IV, a group II metabotropic glutamate receptor agonist that selectively blocks evoked MFT release, to hippocampal slices abolished optically evoked inhibitory and excitatory responses in CA2 pyramidal neurons. We did not detect changes in

oEPSC or oIPSC paired pulse ratios (PPRs) indicating that the vesicle release machinery in MFTs was not affected in *Dyrk1a* $^{+/-}$ mice or following *Ablim3* downregulation in DGCs (Figure 4D).

We next assessed changes in intrinsic excitability of PV INs in CA2 in *Dyrk1a* $^{+/-}$ mice. Current injections in PV INs revealed reduced excitability in *Dyrk1a* $^{+/-}$ mice which was rescued by *Ablim3* downregulation in DGCs (Figure 4E). We did not detect significant differences in passive membrane properties of PV INs between *Dyrk1a* genotypes. However, *Ablim3* downregulation in DGCs reduced the threshold for action potential in PV INs (Figure S6C). These findings suggest that increasing mossy fiber excitatory drive onto PV INs restored intrinsic excitability of these cells.

Taken together, these findings demonstrate that viral *Ablim3* downregulation in DGCs in adulthood reverses *Dyrk1a* heterozygosity-associated developmental impairments in FFI in DG-CA2, CA2 PV IN intrinsic excitability, and GABAergic inhibition in CA2. We next investigated inhibitory synaptic transmission in DG-PV IN-CA3 circuitry in *Dyrk1a* $^{+/-}$ mice.

Ablim3 downregulation in DGCs of adult heterozygous *Dyrk1a* mice restores inhibitory synaptic transmission in DG-CA3

Whole-cell recordings from tdTomato labeled PV INs in CA3 of *Dyrk1a*$^{+/-}$ mice revealed a significant reduction in frequency, but not amplitude, of mEPSCs (Figures 5A-5B, Supplementary Table 1). Consistent with reduced PV IN perisomatic contacts in CA3, we observed a reduction in frequency, but not amplitude, of mIPSCs in CA3 pyramidal neurons (Figure 5C). We did not detect differences in frequency or amplitude of mEPSCs in CA3 pyramidal neurons in *Dyrk1a*$^{+/-}$ mice (Figure S7A). Viral downregulation of *Ablim3* in DGCs of *Dyrk1a* $^{+/-}$ mice completely reversed decrements in frequency of mEPSCs in PV INs in CA3 and frequency of mIPSCs in CA3 pyramidal neurons (Figures 5B-5C).

Next, we asked whether these developmental reductions in excitatory inputs onto PV INs and inhibitory inputs onto CA3 neurons in *Dyrk1a* $^{+/-}$ mice result in reduced DGC recruitment of FFI onto CA3. Analysis of oEPSCs and oIPSCs in CA3 neurons following optogenetic stimulation of mossy fibers revealed a significantly higher excitation-inhibition ratio in *Dyrk1a* $^{+/-}$ mice that was driven by a significant increase in oEPSCs (Figure 5D). Viral expression of *Ablim3* shRNA in DGCs of *Dyrk1a* $^{+/-}$ mice resulted in complete restoration of the excitation-inhibition ratio through a robust increase in oIPSCs and reduction in oEPSCs in CA3 pyramidal neurons. Bath application of DCG-IV to hippocampal slices abolished optically evoked inhibitory and excitatory responses in CA3 pyramidal neurons. We did not detect any changes in oEPSC and oIPSC PPRs in CA3 neurons of *Dyrk1a* $^{+/-}$ mice or following *Ablim3* downregulation in DGCs (Figure 5D).

As with PV INs in CA2, current injections in PV INs in CA3 revealed reduced intrinsic excitability in *Dyrk1a* $^{+/-}$ mice which was rescued by *Ablim3* downregulation in DGCs (Figure 5E). We did not detect significant differences in passive membrane properties of PV INs between *Dyrk1a* genotypes (Figure S7B).

Taken together, these findings demonstrate that viral *Ablim3* downregulation in DGCs in adulthood reverses *Dyrk1a* heterozygosity-associated developmental impairments in FFI in DG-CA3, CA3 PV IN intrinsic excitability and GABAergic inhibition in CA3.

Ablim3 downregulation in DGCs of adult heterozygous *Dyrk1a* mice restores social recognition

To determine if *Dyrk1a* heterozygosity impairs social cognition and whether *Ablim3* downregulation in DGCs may exert restorative effects, we tested adult *Dyrk1a*$^{+/+}$ or *Dyrk1a*$^{+/-}$ littermates expressing shRNA or shNT in DGCs in the social recognition and discrimination task (Figure 6A). *Dyrk1a*$^{+/-}$ mice were impaired in social recognition i.e they spent equivalent amount of time investigating the social stimulus and empty cup in the first trial but learned to distinguish a novel social stimulus from the familiarized social stimulus in trial 4 (Figure 6F, Figure S9C). Viral downregulation of *Ablim3* in DGCs of *Dyrk1a* $^{+/-}$ mice rescued this impairment in social recognition. Analysis of this same cohort of mice in assays for anxiety-like behavior, object preference, and novel object recognition suggested that *Dyrk1a* heterozygosity does not affect behavioral measures and performance in these domains (Figures 6B-6E). Interestingly, developmental deletion of *Dyrk1a* in hippocampus and cortex also produced a similar impairment in social recognition without affecting anxiety-like behavior [10]. Taken together, our findings demonstrate that viral *Ablim3* downregulation in DGCs in adulthood is sufficient to reverse *Dyrk1a* heterozygosity-associated developmental impairments in social recognition.

Acute chemogenetic activation of PV INs in CA3/CA2 of adult *Dyrk1a*$^{+/-}$ mice is sufficient to rescue social recognition

So far, our data identify ABLIM3 and PV IN mediated perisomatic inhibition as molecular and circuit substrates of DYRK1A function in DG-CA3 and DG-CA2 circuits. We next investigated the potential of directly activating PV INs in CA3/CA2 in *Dyrk1a* $^{+/-}$ mice to rescue the social recognition impairment. We performed stereotaxic injections of rAAV-S5E2-hM3D(Gq)DREADD-P2A-dTomato into CA3/CA2 of *Dyrk1a*$^{+/+ \text{ or } +/-}$ mice to express the chemogenetic activator hM3D(Gq)-DREADD [84] exclusively in PV INs (Figure 7A). Using a cross-over CNO/saline design with adult male and female *Dyrk1a* $^{+/+ \text{ or } +/-}$ mice, we found that acute chemogenetic activation of PV INs in CA3/CA2 did not affect anxiety-like behavior, object preference, and novel object recognition (Figures 7B-7D) but was sufficient to rescue social recognition impairments (Figure 7E, Figure S9D). Acute CNO treatment as assessed using *Dyrk1a*$^{+/+}$ mice did not affect anxiety-like behavior, object recognition or social recognition behavior (Figure S8, Figure S9F).

DISCUSSION

Dyrk1a haploinsufficiency is associated with a constellation of somatic, neurological and neurobehavioral symptoms including ASD. A major challenge is understanding how *Dyrk1a* heterozygosity impairs social cognition. Studies in invertebrates and mice have found that *Dyrk1a* LOF mutations affect dendritic arborization, soma size, axonal elongation, dendritic spines, presynaptic terminal growth and synaptic vesicle recycling [6-17,19,85]. Additionally, frameshift mutations in *Dyrk1a* [86] or conditional deletion of *Dyrk1a* in neocortex and

hippocampus [10] impair social recognition in mice. However, despite this knowledge, we do not know how DYRK1A regulates synaptic and circuit functions to influence social cognition. Here, we demonstrate a role for DYRK1A in DGCs in regulating mossy fiber recruitment of PV INs, maintaining PV IN intrinsic excitability and recruiting GABAergic inhibition of CA3 and CA2. We show that acute loss of one functional allele of *Dyrk1a* in DGCs is sufficient to reduce MFT-filopodial contacts with PV INs and PV IN perisomatic contacts in CA3. Global loss of a functional allele of *Dyrk1a* throughout life also resulted in reduced mossy fiber recruitment of PV INs and decreased GABAergic inhibition of CA3 and CA2 without affecting DGC dendritic spine density, PP-DGC synaptic properties or mossy fiber vesicle release probability. Acute loss of a functional allele of *Dyrk1a* in DGCs or global *Dyrk1a* heterozygosity resulted in impaired social recognition. Together, these acute, cell-type specific and global, developmental manipulations of *Dyrk1a* identify a dosage sensitive function for DYRK1A in DGCs in recruiting PV IN mediated GABAergic inhibition in CA3 and CA2 and regulation of social recognition.

In the absence of known activators of DYRK1A function, can we devise strategies to reverse *Dyrk1a* haploinsufficiency-associated reductions in DGC recruitment of FFI of CA3/CA2 and social recognition impairment? Here, we implemented functional epistasis logic to target a downstream effector and synaptic substrate of DYRK1A in mossy fiber terminals, ABLIM3, to achieve this goal. In prior work, we showed that ABLIM3 functions as a molecular brake of DGC mediated FFI in DG-CA3. Here, we generated multiple lines of evidence to demonstrate that ABLIM3 functions downstream of DYRK1A in mossy fibers to recruit FFI in DG-CA2 and DG-CA3. First, we found that heterozygous *Dyrk1a* mice failed to show social experience-dependent ABLIM3 downregulation in mossy fibers. Second, viral expression of an ABLIM3 phosphomimetic mutant (that mimics DYRK1A phosphorylation of ABLIM3) in DGCs of wild-type mice increased MFT-filopodial contacts with PV INs and PV IN perisomatic contacts with CA3/CA2 neurons. Conversely, viral overexpression of an ABLIM3 phospho-dead mutant in DGCs of wild-type mice abolished social experience-induced enhancement in MFT-filopodial contacts with PV INs and PV IN perisomatic contacts with CA3/CA2 neurons and impaired social recognition. Third, we found that viral downregulation of *Ablim3* in DGCs lacking one or both alleles of *Dyrk1a* was sufficient to restore FFI connectivity, PV IN perisomatic contacts and social recognition. Building on these findings, we showed that viral *Ablim3* downregulation in DGCs of adult heterozygous *Dyrk1a* mice was sufficient to restore DGC recruitment of GABAergic inhibition in CA3 and CA2, intrinsic excitability of PV INs and social recognition.

Our study implicates neural activity and more specifically, mossy fiber excitatory inputs, in regulating PV IN mediated perisomatic innervation and GABAergic inhibition of CA3 and CA2 neurons. These observations suggest that PV INs in the adult brain continue to exhibit experience-dependent plasticity of perisomatic inhibition that is observed during sensitive periods of brain development [87-89]. Interestingly, we also found that increasing mossy fiber excitatory drive onto PV INs increased PV IN intrinsic excitability or intrinsic plasticity [88]. Thus, mossy fiber recruitment of FFI in DG-CA3/CA2 circuits may also depend on increased PV IN excitability as shown for FFI in CA3-CA1 circuits [90]. Whether developmental, genetic or epigenetic programs involved in PV IN maturation, excitability and specification of synaptic connectivity are re-used to mediate activity-dependent changes

in PV INs excitability and perisomatic inhibition in DG-CA3/CA2 circuits is to be determined [91-97].

A growing body of work implicates entorhinal cortex-DG-CA3/CA2 circuits in different facets of social cognition such as social recognition, social memory discrimination and consolidation [28-39,43,98-103]. This study causally links a hippocampal circuit mechanism, DGC recruitment of PV mediated inhibition of CA3 and CA2, with social recognition. The behavioral phenotype captured in the social cognition task (often referred to as impaired sociability or social approach or social interaction) suggests impairments in early stages of social recognition or encoding of social stimuli. When presented with a novel social stimulus, mice process sensory social information associated with that stimulus [43], retrieve prior social representations of littermates and cagemates for comparison and assessment of novelty and mismatch, and encode the novel social stimulus as a distinct or updated representation in CA2/CA3 circuits. Loss of *Dyrk1a* in DGCs in adulthood or throughout development potentially impairs this capacity to encode social stimuli by disrupting FFI in DG-CA2 and DG-CA3 resulting in a social recognition impairment. We show that mossy fiber excitatory inputs onto PV INs and PV IN-CA3/CA2 inhibitory circuits are highly sensitive to social experience. Restoration of PV IN mediated inhibition onto CA3 and CA2 by either increasing excitatory drive onto PV INs and enhancing PV IN plasticity (inhibitory contacts with CA3/CA2 neurons) or direct chemogenetic activation of PV INs is sufficient to restore social recognition in adult heterozygous *Dyrk1a* mice. How does PV mediated perisomatic inhibition of CA3/CA2 contribute to social recognition? Perisomatic inhibition of CA3/CA2 neurons may impose a sparse activity regimen that supports generation of distinct neuronal ensembles in response to an experience [44,49-52,59,60,104-106]. Consistent with this idea, DGC recruitment of FFI in CA3/CA2 is randomly wired so as to provide blanket inhibition and govern network excitability in CA3 and CA2, rather than couple individual DGC-dependent excitation with inhibition onto distinct populations of pyramidal neurons [52]. Loss of PV IN mediated inhibition may disrupt neuronal ensembles and network oscillations by impairing neuronal spiking, recurrent excitation in CA3 networks [107], reciprocal inhibition between CA3 and CA2 [35,108-112] and/or the balance between subcortical and entorhinal inputs to CA3/CA2 during encoding of social stimuli [27,28,113,114]. Future studies will edify how PV inhibition of CA3/CA2 facilitates encoding of social stimuli in CA3 and CA2 neuronal ensembles and network oscillations.

Our work exemplifies how functional epistasis logic can be deployed to rescue *Dyrk1a* haploinsufficiency associated circuit and behavioral impairments. Such an approach is advantageous over efforts to identify DYRK1A activators for several reasons. First, screening and identification of activators of kinases is notoriously difficult and currently, there are no known chemical activators of DYRK1A. Thus, targeting specific DYRK1A substrates in distinct somatic, neuronal and non-neuronal cell-types that mediate different DYRK1A functions in physiology and behavior may represent a more viable approach. Second, ABLIM3, like other DYRK1A substrates shows greater cell-type and tissue restricted expression than DYRK1A. Consequently, targeting DYRK1A substrates may permit rescue of subsets of somatic and neurological endophenotypes that make up syndromic ASD while reducing risk of cancer malignancies and neuropathology associated with widespread DYRK1A overactivation [7,11,115,116].

While it remains challenging to precisely determine how *Dyrk1a* haploinsufficiency affects the trajectory of brain development or for that matter, restore the arc of "normal" development, our work illuminates the potential for targeting DYRK1A synaptic substrates in adulthood to alleviate the burden of developmentally accrued impairments in circuitry and cognition associated with *Dyrk1a* haploinsufficiency. Indeed, a small but growing number of studies support the promise of restoring functions in neurodevelopmental disorders after sensitive periods of brain development [117-120]. The last few years has witnessed the emergence of gene therapy as a potential therapeutic modality for neurological and psychiatric diseases [121]. This paradigm shift in thinking and approach to brain diseases has been catalyzed by advances in directed capsid evolution and AAV engineering, cell-type specific payload expression such as that shown here for PV INs [82], antisense oligo and siRNA delivery (intrathecal delivery and intravenous) and gene delivery modalities [122-128]. Targeting molecular effectors of DYRK1A such as ABLIM3 using antisense oligo, siRNA (cell-type specific [129]) or intrathecally delivered to avoid ABLIM3 in muscle, or viral shRNA gene therapy (directly into hippocampus) or viral mediated enhancement of PV IN mediated inhibition of CA3/CA2 may harbor potential for ameliorating social recognition impairments associated with *Dyrk1a* haploinsufficiency and potentially, other neurodevelopmental disorders characterized by deficits in FFI in DG-CA3/CA2 circuits and PV IN dysfunction [2,93,130].

STAR METHODS

RESOURCE AVAILABILITY

Lead Contact—Further information and requests for resources and reagents should be directed to and will be fulfilled by the Lead Contact, Dr.Amar Sahay (asahay@mgh.harvard.edu).

Materials Availability—Plasmids generated as part of this study (specific to *Dyrk1a* and *Ablim3*) will be shared upon request.

Data and code Availability

- Plasmids generated as part of this study (specific to *Dyrk1a* and *Ablim3*) will be shared upon request.
- Microscopy, electrophysiology and behavior data reported in this paper will be shared by the lead contact upon request.
- Any additional information required to reanalyze the data reported in this paper is available from the lead contact upon request.

EXPERIMENTAL MODEL DETAILS

Animals—All mice were group housed and experiments were conducted in accordance with procedures approved by the Institutional Animal Care and Use Committees at the Massachusetts General Hospital and NIH guidelines (IACUC 2011N000084). All mice were housed in a 12-h (7 a.m. to 7 p.m.) light–dark colony room at 22–24 °C with *ad libitum* access to food and water. Adult female mice (3–4 months old) were purchased

from the Jackson Laboratories for breeding. Mouse lines were obtained from the Jackson Laboratories and details are provided in the resource table.

METHOD DETAILS

Viruses and virus constructs—Lenti-shNT and shRNA (*Ablim3*) viruses were generated in the laboratory as described previously (Guo et al., 2018). rAAV viruses were purchased from Addgene. Lenti-shNT-Ubi-Cre-T2A-GFP and shRNA-Ubi-Cre-T2A-GFP (*Ablim3*) constructs were generated by subcloning Cre-T2A-GFP from plasmid-CamKIIα-Cre-T2A-GFP (VectorBuilder) into lenti-shNT and shRNA (*Ablim3*) plasmids. Lenti-ABLIM3-SD and SA mutant (S408; protein accession number AAH60275) constructs were generated in the laboratory using the lenti-ABLIM3 plasmid as a template [44] and QuikChange II site-directed mutagenesis kit (Agilent). Lentiviruses were produced by cotransfection of lenti vectors and packaging plasmids into HEK293T cells. Briefly, 24 hours following transfection, the supernatant was collected every day for 3 days. The supernatant was concentrated by ultra- centrifugation. Virus pellets were resuspended overnight in Dulbecco's phosphate-buffered saline (DPBS)[44].

Stereotactic viral injection—Mice received carprofen (5mg/kg subcutaneously, Patterson Veterinary Supply) before surgery and were then anaesthetized with ketamine and xylazine (10 mg/ml and 1.6 mg/ml, IP). Mice were placed in the stereotaxic apparatus, and a small hole was drilled at each injection location (Foredom K.1070 High Speed Rotary Micromotor Kit). Bilateral injections were performed using Hamilton microsyringes (Hamilton, Neuros Syringe 7001) that were slowly lowered into target sites and that were left there for 8 min prior to infusion at a rate of 0.1 μl/min. The coordinates relative to bregma: dorsal DG: −1.8 mm (AP), ±1.35 mm (ML), −2.25 mm (DV) and dorsal CA2/CA3: −1.8 mm (AP), ±2.45 mm (ML), −2.35 mm (DV). The microsyringes were slowly withdrawn after infusion and the skin above the incision was sutured with coated vicryl sutures (Ethicon US LLC). Mice were monitored and received a daily injection of carprofen (5 mg/kg, i.p) for 3 days following surgery [49].

Tissue collection and qRT-PCR analysis—Hippocampal DG regions were harvested and snap-frozen. Briefly, cDNA samples made from RNA collected from *EIIaCre:Dyrk1a*$^{+/+}$ and *EIIaCre:Dyrk1a1*$^{f/+}$ mice or WT mice with either lenti-shNT or shRNA (*Ablim3*) injection into DG. Total RNA was quantified using a NanoDrop spectrophotometer (Thermo Scientific) and then equal amounts of RNA were used for reverse transcription (Superscript IV First-strand synthesis system, Invitrogen). qRT-PCR was carried out with SYBR green (BioRad) and primers (Primer bank)[131] with following sequences: *Ablim1*-F 5'- CAACATTTACCGAAAACCACCC; *Ablim1*-R 5'- GCTGCTGGGAACTTGGAAAA; *Ablim2*-F 5'- AACCTGACACTCTTCCAGGAC; *Ablim2*R 5'- TTTGGGCAGTTTCACACGAAT; *Ablim3*-F 5'-GGTCCGTGTCCACAACAAC; *Ablim3*-R 5'- GTCCCGGCAGCTATCACAG; *Dyrk1a*-F 5'- GAAGCGAAGACACCAACAGG; *Dyrk1a*-R 5'-ACCCATTCTTGCTCCACTCT; *Gapdh*-F 5'- GCTTGTCATCAACGGGAAG; *Gapdh*-R 5'-TTGTCATATTTCTCGTGGTTCA.

Behavioral procedures—Two weeks after viral injections, mice were handled for 3 days prior to behavioral experiments to habituate them to human handling and transportation from vivarium to behavioral testing rooms. For chemogenetic actuation of PV INs, mice were habituated to an empty syringe for 3 days and then CNO (1mg/kg) was injected 30 min prior to experiments. The behavioral assays were performed in the following order: open-field (OF, day 1), light-dark test (day 2), object recognition (OR, day 3), novel object recognition (NOR, day 4), and social recognition and discrimination (day 6). For assessing effects of context vs social experience on FFI connectivity, mice were habituated to the behavioral chamber for 7 days. All the behavioral assays were performed in the same chambers (40 × 40 cm, MazeEngineers). Videos were recorded and exported from Freezeframe (Actimetrics) and analyzed with EthoVision XT 15 (Noldus). Center point tracking was used to record movement and nose point tracking was used to evaluate object and social interaction. An interaction was considered when the test mouse's nose position to object or stimulus mouse was within 1 cm [44,49].

Open-field paradigm—Mice were transported into a holding room and habituated for one hour prior to testing. Total distance traveled and the time spent in the center of the arena were quantified over 30 min [44].

Light-Dark task—A dark opaque box (40 x 20 cm) with an opening in the center of one wall was placed in the OF chamber to create light (150 lux) and dark compartments of equal size. The mouse was placed in the light compartment and allowed to explore freely for 10 min. Time spent and distance traveled in the light compartment was recorded [34,44].

Object recognition—One object (4 x 4 x 6 cm) was placed in the OF chamber along one side (5 cm distance from the wall). Mice were placed in the opposite side of the object and allowed to explore freely for 5 min. Time spent exploring the object (noise point within 2 cm) was quantified [44].

Novel object recognition—One object (2 x 4 x 6 cm) was placed in the OF chamber along one corner and the other one was placed in the opposite corner (2 x 2 x 10 cm, 5 cm distance from the wall). The mouse was placed in the center and allowed to explore freely for 5 min. Time spent exploring the objects (nose point within 2 cm) were quantified [34,44].

Social recognition, familiarization and social discrimination—Stimulus mice (strain, age and sex-matched) were habituated to being placed in a pencil wire cup in the OF chamber prior to the task day for 3 days, 15 min per day. The task consisted of 3 trials for familiarization and one trial for discrimination with 5 min intertrial intervals. For trial 1 (early stages of social encoding/social recognition), subjects were placed in the center of the chamber for 10 min with two pencil wire cups placed on opposite corners. A beaker was placed above the pencil cup to prevent subject from climbing on the top. One cup contained a stimulus mouse; the other one remained empty. Subjects were trained from trial 1 (social recognition) to trial 3 to familiarize the stimulus mouse with the test mouse. The locations of the stimulus and empty cup were counterbalanced across trials. On trial 4 (discrimination), a novel stimulus mouse was added to the empty cup. Time spent exploring the empty and stimulus mouse were quantified (nose point within 1 cm)(Raam et al., 2017).

The immediate social recognition task consisted of 3 trials: habituation (empty vs empty), recognition (empty vs stimulus), and discrimination (novel vs familiar).

Immunohistochemistry—Mice were anaesthetized with ketamine and xylazine (10 mg/ml and 1.6 mg/ml, IP), transcardially perfused with 4% PFA, and brains were incubated in 4% PFA at 4°C overnight. Brains were placed in 30% sucrose/PBS for 2 days and then embedded in medium (OCT, Fisher Healthcare). 35 μm cryosections were obtained (Leica) and stored in PBS (0.01% sodium azide) at 4°C. For immunostaining, floating sections were permeabilized, blocked in blocking solution for 2 h (PBS containing 0.3 % Triton X-100 and 10% normal donkey serum, NDS), and followed by incubation with primary antibodies (PBS containing 10% NDS) at 4°C overnight. Sections were then washed with PBS 3 times, 10 min each, followed by incubated with secondary antibodies in PBS for 2 h at room temperature (RT). Sections were then washed with PBS 3 times, 10 min each, mounted on glass slides and cover slipped with mounting medium containing DAPI. For DYRK1A and ABLIM3 immunostaining, brains were rapidly removed and flash frozen. 20 μm cryosections were mounted on glass slides, air-dried, and fixed in 95% ethanol immediately at −20°C for 30 min, followed by 100% acetone for 1 min at RT. Slides were rinsed with PBS, blocked with 1% BSA for 30 min, then incubated with primary antibodies (in blocking buffer) for 2 h. Slides were washed with PBS 3 times, 5 min each, sections were incubated with secondary antibodies (in PBS) for 30 min. Finally, sections were washed with PBS 3 times, 5 min each, and cover slipped with mounting medium containing DAPI. See Key Resource Table for primary antibodies information and dilutions.

Image analysis of mossy fiber terminals, PV puncta and dendritic spines—Images were obtained from 6 sections per mouse hippocampus blind to treatment and genotype. A Leica SP8 confocal laser microscope and LAS software were used to capture images in the stratum lucidum at high-resolution (2,048). For MFTs, images were captured in the CA3ab subfield with a 0.3 μm step size of *z*-stacks using a 63× oil objective plus 6× digital zoom. MFT filopodia were defined as protrusions longer than 1 μm with an end-swelling structure; for PV puncta, single confocal plane images were captured in the CA2 and CA3ab subfields using a 63× oil objective plus 4× digital zoom. For dendritic spines, images were captured in the outer one-third of the molecular layer of the DG with a 0.3 μm step size of *z*-stacks using a 63× oil objective plus 4× digital zoom, then processed with the maximum-intensity projection using FIJI ImageJ. Quantification sample size: for filopodia numbers per MFT, 20-30 MFTs were collected per mouse; for PV puncta, density was averaged from 18 images per mouse; for dendritic spine densities, 20-30 dendrites were collected per mouse[44,49]. PV puncta was analyzed using the StarDist 2D plugin and particle analysis tools in FIJI ImageJ. Threshold values were held constant across images.

Ex vivo electrophysiology—Mice were unilaterally injected with 0.4 μL lenti-*Ablim3*-shRNA/shNT and 0.3 μL AAV5-CamKII-ChR2-eYFP into the dorsal DG, and 0.3 μL AAV-S5E2-tdTomato into dorsal CA3/CA2 of 8-week-old mice (see above for stereotactic coordinates). At 2-3 weeks after viral infusion, mice were anaesthetized with ketamine and xylazine (10 mg/ml and 1.6 mg/ml, IP) then transcardially perfused with ice-cold (4 oC) choline chloride-based artificial cerebrospinal fluid (ACSF) composed of (in mM): 92

choline chloride, 2.5 KCl, 1.25 NaH_2PO_4, 30 $NaHCO_3$, 20 HEPES, 25 glucose, and 10 $MgSO_4 \cdot 7H_2O$. Their brains were rapidly extracted following decapitation. Coronal slices (300 μm thick) containing the dorsal hippocampus were cut in ice-cold (4 oC) choline chloride ACSF using a Leica VT1000 vibratome (Leica Biosystems) and transferred to warm (33 °C) normal ACSF for 30 min. Normal ACSF contained (in mM): 124 NaCl, 2.5 KCl, 1.25 NaH_2PO_4, 24 $NaHCO_3$, 5 HEPES, 12.5 glucose, 2 $MgSO_4 \cdot 7H_2O$, 2 $CaCl_2 \cdot 2H_2O$. All ACSF solutions were adjusted to a pH of 7.4, mOsm of 305, and were saturated with carbogen (95% O_2 and 95% CO_2). Slices were allowed to cool to room temperature (20-22 oC) for 1 hour before recordings.

Whole-cell patch-clamp recordings were obtained using a Multiclamp 700B amplifier (Molecular Devices) low-pass filtered at 1.8 kHz with a four-pole Bessel filter and digitized with a Digidata 1550B (Molecular Devices). Slices were placed in a submersion chamber and continually perfused (>2 mL/min) with normal ACSF. Neurons were visually identified by infrared differential interference contrast imaging combined with epifluorescence using LED illumination (pE-300white, CoolLED). Pyramidal neurons in CA2 and CA3ab were distinguished by their anatomical location and distinct electrophysiological properties (Chevaleyre and Siegelbaum, 2010). Borosilicate patch pipettes had an impedance of 4-5 MΩ and filled with an internal solution containing (in mM): 120 CsMeS, 4 $MgCl_2$, 1 EGTA, 10 HEPES, 5 QX- 314, 0.4 Na_3GTP, 4 MgATP, 10 phosphocreatine, 2.6 biocytin, pH 7.3, 290 mOsm. For miniature inhibitory postsynaptic current recordings, patch pipettes were filled with 140 mM CsCl in place of CsMeS. For current-clamp recordings, patch pipettes were filled with 130 mM potassium gluconate in place of CsMeS with QX-314 excluded. Once GΩ seal was obtained, neurons were held in voltage-clamp configuration at −70 mV and the input resistance, resting membrane potential, and capacitance were measured. Series resistance (<30 MΩ) was monitored throughout recordings and recordings were discarded if series resistance changed by >20% from baseline.

For electrically evoked EPSCs and IPSCs from DG, a concentric bipolar tungsten electrode was used to deliver electrical stimulation (0.2 ms duration) in the molecular layer of the DG. Electrically-evoked current responses were recorded at 1.5-fold threshold, defined as the minimum stimulation intensity required to produce a consistent current response beyond baseline noise.

For optically evoked EPSCs and IPSCs, 2 ms 473 light pulses were delivered above the mossy fiber pathway – the hilus of the DG. Current responses were recorded at 1.5-fold threshold.

For current clamp recordings of PV INs, bursting neurons, identified by their asynchronous rapid firing within the first 50 ms of the current step followed by failure to fire, were excluded from analysis. For miniature postsynaptic current recordings, 1 μM tetrodotoxin was included in the bath ACSF. Kynurenic acid 2mM was included when recording mIPSCs and 0.1 mM picrotoxin when recording mEPSCs. Autodetection parameters for inclusion of events was determined by calculating minimum threshold: root mean square (RMS)2 × 1.5. To control for oversampling and unequal sample size between groups, quantile sampling of the frequency and amplitude was calculated by computing 29 evenly spaced quantile values

from each neuron, starting at 1 percentile and ending at 94.2 percentile, with a step size of 3.33%[132]. Data acquisition was performed using Clampex and analyzed with Clampfit (Molecular Devices). EasyElectrophysiology software (V2.4.1) was used to analyze mPSC recordings.

Sex as a biological variable—Sex of all mice was factored into design and analyses. If no statistical difference or interaction between sex were observed, then mice were grouped and analyzed according to experimental condition.

QUANTIFICATION AND STATISTICAL ANALYSIS

We adhered to accepted standards for rigorous study design and reporting to maximize the reproducibility and translational potential of our findings as described in [133] and in ARRIVE Guidelines[134]. All experimenters were blind to treatment conditions throughout data collection, scoring, and analyses. Statistical analyses were conducted using Prism v9 (GraphPad) and the minimum sample size was determined based on prior experience, existing literature, and a power analysis. Statistical significance was defined as $p < 0.05$. Two-tailed Student's t-tests were used for two-group comparisons. Analysis of variance (ANOVA) were used for three or more group comparisons. Repeated-measures ANOVA were used for comparison of groups across treatment condition or time. Appropriate nonparametric tests were used when data sets failed to meet parametric assumptions. Detailed statistical analyses can be found in Table S1.

Supplementary Material

Refer to Web version on PubMed Central for supplementary material.

ACKNOWLEDGEMENTS

We thank members of Sahay lab, L.M.S. Sahay and L.B.B. Sahay for comments on the manuscript. Y.S. was supported by MGH ECOR Fund for Medical Discovery (FMD) Fundamental Research Fellowship Award and is recipient of a Harvard Brain Initiative Travel Grant. A.S. acknowledges support from NIH R01MH111729, R01MH131652, R01MH111729-04S1, R01AG076612, R01AG076612-S1 diversity supplement, The Simons Collaboration on Plasticity and the Aging Brain, James and Audrey Foster MGH Research Scholar Award and MGH department of Psychiatry. A.S dedicates this study to the late Michael Mishkind, Ph.D. for his unwavering guidance and mentorship at Bennington College and to Kushal "Tiche" Sacheti for investing in the science of curiosity.

INCLUSION AND DIVERSITY

We worked to ensure sex balance in the selection of non-human subjects. One or more of the authors of this paper self-identifies as an underrepresented ethnic minority in science. One or more of the authors of this paper received support from a program designed to increase minority representation in science. While citing references scientifically relevant for this work, we also actively worked to promote gender balance in our reference list. The author list of this paper includes contributors from the location where the research was conducted who participated in the data collection, design, analysis, and/or interpretation of the work.

REFERENCES

1. Lord C, Brugha TS, Charman T, Cusack J, Dumas G, Frazier T, Jones EJH, Jones RM, Pickles A, State MW, et al. (2020). Autism spectrum disorder. Nat Rev Dis Primers 6, 5. 10.1038/s41572-019-0138-4. [PubMed: 31949163]
2. Willsey HR, Willsey AJ, Wang B, and State MW (2022). Genomics, convergent neuroscience and progress in understanding autism spectrum disorder. Nat Rev Neurosci 23, 323–341. 10.1038/s41583-022-00576-7. [PubMed: 35440779]
3. O'Roak BJ, Vives L, Fu W, Egertson JD, Stanaway IB, Phelps IG, Carvill G, Kumar A, Lee C, Ankenman K, et al. (2012). Multiplex targeted sequencing identifies recurrently mutated genes in autism spectrum disorders. Science 338, 1619–1622. 10.1126/science.1227764. [PubMed: 23160955]
4. Earl RK, Turner TN, Mefford HC, Hudac CM, Gerdts J, Eichler EE, and Bernier RA (2017). Clinical phenotype of ASD-associated DYRK1A haploinsufficiency. Molecular autism 8, 54. 10.1186/s13229-017-0173-5. [PubMed: 29034068]
5. Satterstrom FK, Kosmicki JA, Wang J, Breen MS, De Rubeis S, An JY, Peng M, Collins R, Grove J, Klei L, et al. (2020). Large-Scale Exome Sequencing Study Implicates Both Developmental and Functional Changes in the Neurobiology of Autism. Cell 180, 568–584 e523. 10.1016/j.cell.2019.12.036. [PubMed: 31981491]
6. Arranz J, Balducci E, Arato K, Sanchez-Elexpuru G, Najas S, Parras A, Rebollo E, Pijuan I, Erb I, Verde G, et al. (2019). Impaired development of neocortical circuits contributes to the neurological alterations in DYRK1A haploinsufficiency syndrome. Neurobiol Dis 127, 210–222. 10.1016/j.nbd.2019.02.022. [PubMed: 30831192]
7. Souchet B, Guedj F, Sahun I, Duchon A, Daubigney F, Badel A, Yanagawa Y, Barallobre MJ, Dierssen M, Yu E, et al. (2014). Excitation/inhibition balance and learning are modified by Dyrk1a gene dosage. Neurobiol Dis 69, 65–75. 10.1016/j.nbd.2014.04.016. [PubMed: 24801365]
8. Soppa U, and Becker W (2015). DYRK protein kinases. Curr Biol 25, R488–489. 10.1016/j.cub.2015.02.067. [PubMed: 26079075]
9. Duchon A, and Herault Y (2016). DYRK1A, a Dosage-Sensitive Gene Involved in Neurodevelopmental Disorders, Is a Target for Drug Development in Down Syndrome. Front Behav Neurosci 10, 104. 10.3389/fnbeh.2016.00104. [PubMed: 27375444]
10. Levy JA, LaFlamme CW, Tsaprailis G, Crynen G, and Page DT (2021). Dyrk1a Mutations Cause Undergrowth of Cortical Pyramidal Neurons via Dysregulated Growth Factor Signaling. Biol Psychiatry 90, 295–306. 10.1016/j.biopsych.2021.01.012 [PubMed: 33840455]
11. Thompson BJ, Bhansali R, Diebold L, Cook DE, Stolzenburg L, Casagrande AS, Besson T, Leblond B, Desire L, Malinge S, and Crispino JD (2015). DYRK1A controls the transition from proliferation to quiescence during lymphoid development by destabilizing Cyclin D3. The Journal of experimental medicine 212, 953–970. 10.1084/jem.20150002. [PubMed: 26008897]
12. Atas-Ozcan H, Brault V, Duchon A, and Herault Y (2021). Dyrk1a from Gene Function in Development and Physiology to Dosage Correction across Life Span in Down Syndrome. Genes (Basel) 12. 10.3390/genes12111833.
13. Classen J, Saarloos I, Meijer M, Sullivan PF, and Verhage M (2020). A Munc18-1 mutant mimicking phosphorylation by Down Syndrome-related kinase Dyrk1a supports normal synaptic transmission and promotes recovery after intense activity. Scientific reports 10, 3181. 10.1038/s41598-020-59757-y. [PubMed: 32081899]
14. Benavides-Piccione R, Dierssen M, Ballesteros-Yanez I, Martinez de Lagran M, Arbones ML, Fotaki V, DeFelipe J, and Elston GN (2005). Alterations in the phenotype of neocortical pyramidal cells in the Dyrk1A+/− mouse. Neurobiol Dis 20, 115–122. 10.1016/j.nbd.2005.02.004. [PubMed: 16137572]
15. Dang T, Duan WY, Yu B, Tong DL, Cheng C, Zhang YF, Wu W, Ye K, Zhang WX, Wu M, et al. (2018). Autism-associated Dyrk1a truncation mutants impair neuronal dendritic and spine growth and interfere with postnatal cortical development. Mol Psychiatry 23, 747–758. 10.1038/mp.2016.253. [PubMed: 28167836]

16. Chen CK, Bregere C, Paluch J, Lu JF, Dickman DK, and Chang KT (2014). Activity-dependent facilitation of Synaptojanin and synaptic vesicle recycling by the Minibrain kinase. Nature communications 5, 4246. 10.1038/ncomms5246.

17. Vidaki M, Drees F, Saxena T, Lanslots E, Taliaferro MJ, Tatarakis A, Burge CB, Wang ET, and Gertler FB (2017). A Requirement for Mena, an Actin Regulator, in Local mRNA Translation in Developing Neurons. Neuron 95, 608–622 e605. 10.1016/j.neuron.2017.06.048. [PubMed: 28735747]

18. Guedj F, Pereira PL, Najas S, Barallobre MJ, Chabert C, Souchet B, Sebrie C, Verney C, Herault Y, Arbones M, and Delabar JM (2012). DYRK1A: a master regulatory protein controlling brain growth. Neurobiol Dis 46, 190–203. 10.1016/j.nbd.2012.01.007. [PubMed: 22293606]

19. Falkovich R, Danielson EW, Perez de Arce K, Wamhoff EC, Strother J, Lapteva AP, Sheng M, Cottrell JR, and Bathe M (2023). A synaptic molecular dependency network in knockdown of autism- and schizophrenia-associated genes revealed by multiplexed imaging. Cell reports 42, 112430. 10.1016/j.celrep.2023.112430. [PubMed: 37099425]

20. Avery L, and Wasserman S (1992). Ordering gene function: the interpretation of epistasis in regulatory hierarchies. Trends Genet 8, 312–316. 10.1016/0168-9525(92)90263-4. [PubMed: 1365397]

21. Domingo J, Baeza-Centurion P, and Lehner B (2019). The Causes and Consequences of Genetic Interactions (Epistasis). Annu Rev Genomics Hum Genet 20, 433–460. 10.1146/annurev-genom-083118-014857. [PubMed: 31082279]

22. Woods NI, Stefanini F, Apodaca-Montano DL, Tan IMC, Biane JS, and Kheirbek MA (2020). The Dentate Gyrus Classifies Cortical Representations of Learned Stimuli. Neuron 107, 173–184 e176. 10.1016/j.neuron.2020.04.002. [PubMed: 32359400]

23. Tavares RM, Mendelsohn A, Grossman Y, Williams CH, Shapiro M, Trope Y, and Schiller D (2015). A Map for Social Navigation in the Human Brain. Neuron 87, 231–243. 10.1016/j.neuron.2015.06.011. [PubMed: 26139376]

24. Montagrin A, Saiote C, and Schiller D (2018). The social hippocampus. Hippocampus 28, 672–679. 10.1002/hipo.22797. [PubMed: 28843041]

25. Schafer M, and Schiller D (2018). Navigating Social Space. Neuron 100, 476–489. 10.1016/j.neuron.2018.10.006. [PubMed: 30359610]

26. Schafer M, and Schiller D (2018). The Hippocampus and Social Impairment in Psychiatric Disorders. Cold Spring Harb Symp Quant Biol 83, 105–118. 10.1101/sqb.2018.83.037614. [PubMed: 30787048]

27. Lopez-Rojas J, de Solis CA, Leroy F, Kandel ER, and Siegelbaum SA (2022). A direct lateral entorhinal cortex to hippocampal CA2 circuit conveys social information required for social memory. Neuron 110, 1559–1572 e1554. 10.1016/j.neuron.2022.01.028. [PubMed: 35180391]

28. Chen S, He L, Huang AJY, Boehringer R, Robert V, Wintzer ME, Polygalov D, Weitemier AZ, Tao Y, Gu M, et al. (2020). A hypothalamic novelty signal modulates hippocampal memory. Nature 586, 270–274. 10.1038/s41586-020-2771-1. [PubMed: 32999460]

29. Oliva A, Fernandez-Ruiz A, Buzsaki G, and Berenyi A (2016). Role of Hippocampal CA2 Region in Triggering Sharp-Wave Ripples. Neuron 91, 1342–1355. 10.1016/j.neuron.2016.08.008. [PubMed: 27593179]

30. Oliva A, Fernandez-Ruiz A, Leroy F, and Siegelbaum SA (2020). Hippocampal CA2 sharp-wave ripples reactivate and promote social memory. Nature 587, 264–269. 10.1038/s41586-020-2758-y. [PubMed: 32968277]

31. Alexander GM, Brown LY, Farris S, Lustberg D, Pantazis C, Gloss B, Plummer NW, Jensen P, and Dudek SM (2018). CA2 neuronal activity controls hippocampal low gamma and ripple oscillations. eLife 7. 10.7554/eLife.38052.

32. Alexander GM, Farris S, Pirone JR, Zheng C, Colgin LL, and Dudek SM (2016). Social and novel contexts modify hippocampal CA2 representations of space. Nature communications 7, 10300. 10.1038/ncomms10300.

33. Lin YT, Hsieh TY, Tsai TC, Chen CC, Huang CC, and Hsu KS (2018). Conditional Deletion of Hippocampal CA2/CA3a Oxytocin Receptors Impairs the Persistence of Long-Term Social

Recognition Memory in Mice. J Neurosci 38, 1218–1231. 10.1523/JNEUROSCI.1896-17.2017. [PubMed: 29279308]

34. Raam T, McAvoy KM, Besnard A, Veenema AH, and Sahay A (2017). Hippocampal oxytocin receptors are necessary for discrimination of social stimuli. Nature communications 8, 2001. 10.1038/s41467-017-02173-0.
35. Lehr AB, Kumar A, Tetzlaff C, Hafting T, Fyhn M, and Stober TM (2021). CA2 beyond social memory: Evidence for a fundamental role in hippocampal information processing. Neurosci Biobehav Rev 126, 398–412. 10.1016/j.neubiorev.2021.03.020. [PubMed: 33775693]
36. Stevenson EL, and Caldwell HK (2014). Lesions to the CA2 region of the hippocampus impair social memory in mice. Eur J Neurosci 40, 3294–3301. 10.1111/ejn.12689. [PubMed: 25131412]
37. Finlay JM, Dunham GA, Isherwood AM, Newton CJ, Nguyen TV, Reppar PC, Snitkovski I, Paschall SA, and Greene RW (2015). Effects of prefrontal cortex and hippocampal NMDA NR1-subunit deletion on complex cognitive and social behaviors. Brain Res 1600, 70–83. 10.1016/j.brainres.2014.10.037. [PubMed: 25452020]
38. Hitti FL, and Siegelbaum SA (2014). The hippocampal CA2 region is essential for social memory. Nature 508, 88–92. 10.1038/nature13028. [PubMed: 24572357]
39. Meira T, Leroy F, Buss EW, Oliva A, Park J, and Siegelbaum SA (2018). A hippocampal circuit linking dorsal CA2 to ventral CA1 critical for social memory dynamics. Nature communications 9, 4163. 10.1038/s41467-018-06501-w.
40. Gangopadhyay P, Chawla M, Dal Monte O, and Chang SWC (2021). Prefrontal-amygdala circuits in social decision-making. Nat Neurosci 24, 5–18. 10.1038/s41593-020-00738-9. [PubMed: 33169032]
41. Cope EC, Zych AD, Katchur NJ, Waters RC, Laham BJ, Diethorn EJ, Park CY, Meara WR, and Gould E (2022). Atypical perineuronal nets in the CA2 region interfere with social memory in a mouse model of social dysfunction. Mol Psychiatry 27, 3520–3531. 10.1038/s41380-021-01174-2. [PubMed: 34183768]
42. Tuncdemir SN, Grosmark AD, Turi GF, Shank A, Bowler JC, Ordek G, Losonczy A, Hen R, and Lacefield CO (2022). Parallel processing of sensory cue and spatial information in the dentate gyrus. Cell reports 38, 110257. 10.1016/j.celrep.2021.110257. [PubMed: 35045280]
43. Hassan SI, Bigler S, and Siegelbaum SA (2023). Social odor discrimination and its enhancement by associative learning in the hippocampal CA2 region. Neuron. 10.1016/j.neuron.2023.04.026.
44. Guo N, Soden ME, Herber C, Kim MT, Besnard A, Lin P, Ma X, Cepko CL, Zweifel LS, and Sahay A (2018). Dentate granule cell recruitment of feedforward inhibition governs engram maintenance and remote memory generalization. Nat Med 24, 438–449. 10.1038/nm.4491. [PubMed: 29529016]
45. Acsady L, Kamondi A, Sik A, Freund T, and Buzsaki G (1998). GABAergic cells are the major postsynaptic targets of mossy fibers in the rat hippocampus. J Neurosci 18, 3386–3403. [PubMed: 9547246]
46. Caroni P (2015). Inhibitory microcircuit modules in hippocampal learning. Curr Opin Neurobiol 35, 66–73. 10.1016/j.conb.2015.06.010. [PubMed: 26176433]
47. Ruediger S, Spirig D, Donato F, and Caroni P (2012). Goal-oriented searching mediated by ventral hippocampus early in trial-and-error learning. Nat Neurosci 15, 1563–1571. 10.1038/nn.3224. [PubMed: 23001061]
48. Ruediger S, Vittori C, Bednarek E, Genoud C, Strata P, Sacchetti B, and Caroni P (2011). Learning-related feedforward inhibitory connectivity growth required for memory precision. Nature 473, 514–518. 10.1038/nature09946. [PubMed: 21532590]
49. Twarkowski H, Steininger V, Kim MJ, and Sahay A (2022). A dentate gyrus-CA3 inhibitory circuit promotes evolution of hippocampal-cortical ensembles during memory consolidation. eLife 11. 10.7554/eLife.70586.
50. Mori M, Gahwiler BH, and Gerber U (2007). Recruitment of an inhibitory hippocampal network after bursting in a single granule cell. Proc Natl Acad Sci U S A 104, 7640–7645. 10.1073/pnas.0702164104. [PubMed: 17438288]

51. Torborg CL, Nakashiba T, Tonegawa S, and McBain CJ (2010). Control of CA3 output by feedforward inhibition despite developmental changes in the excitation-inhibition balance. J Neurosci 30, 15628–15637. 10.1523/JNEUROSCI.3099-10.2010. [PubMed: 21084618]
52. Neubrandt M, Olah VJ, Brunner J, and Szabadics J (2017). Feedforward inhibition is randomly wired from individual granule cells onto CA3 pyramidal cells. Hippocampus 27, 1034–1039. 10.1002/hipo.22763. [PubMed: 28696588]
53. Pelkey KA, Chittajallu R, Craig MT, Tricoire L, Wester JC, and McBain CJ (2017). Hippocampal GABAergic Inhibitory Interneurons. Physiol Rev 97, 1619–1747. 10.1152/physrev.00007.2017. [PubMed: 28954853]
54. Hu H, Gan J, and Jonas P (2014). Interneurons. Fast-spiking, parvalbumin(+) GABAergic interneurons: from cellular design to microcircuit function. Science 345, 1255263. 10.1126/science.1255263. [PubMed: 25082707]
55. Gan J, Weng SM, Pernia-Andrade AJ, Csicsvari J, and Jonas P (2016). Phase-Locked Inhibition, but Not Excitation, Underlies Hippocampal Ripple Oscillations in Awake Mice In Vivo. Neuron. 10.1016/j.neuron.2016.12.018.
56. Amilhon B, Huh CY, Manseau F, Ducharme G, Nichol H, Adamantidis A, and Williams S (2015). Parvalbumin Interneurons of Hippocampus Tune Population Activity at Theta Frequency. Neuron 86, 1277–1289. 10.1016/j.neuron.2015.05.027. [PubMed: 26050044]
57. Klausberger T, Magill PJ, Marton LF, Roberts JD, Cobden PM, Buzsaki G, and Somogyi P (2003). Brain-state- and cell-type-specific firing of hippocampal interneurons in vivo. Nature 421, 844–848. 10.1038/nature01374. [PubMed: 12594513]
58. Sohal VS, Zhang F, Yizhar O, and Deisseroth K (2009). Parvalbumin neurons and gamma rhythms enhance cortical circuit performance. Nature 459, 698–702. 10.1038/nature07991. [PubMed: 19396159]
59. Csicsvari J, Hirase H, Mamiya A, and Buzsaki G (2000). Ensemble patterns of hippocampal CA3-CA1 neurons during sharp wave-associated population events. Neuron 28, 585–594. 10.1016/s0896-6273(00)00135-5. [PubMed: 11144366]
60. de la Prida LM, Huberfeld G, Cohen I, and Miles R (2006). Threshold behavior in the initiation of hippocampal population bursts. Neuron 49, 131–142. 10.1016/j.neuron.2005.10.034. [PubMed: 16387645]
61. Buzsaki G (2015). Hippocampal sharp wave-ripple: A cognitive biomarker for episodic memory and planning. Hippocampus 25, 1073–1188. 10.1002/hipo.22488. [PubMed: 26135716]
62. Cardin JA, Carlen M, Meletis K, Knoblich U, Zhang F, Deisseroth K, Tsai LH, and Moore CI (2009). Driving fast-spiking cells induces gamma rhythm and controls sensory responses. Nature 459, 663–667. 10.1038/nature08002. [PubMed: 19396156]
63. Ognjanovski N, Schaeffer S, Wu J, Mofakham S, Maruyama D, Zochowski M, and Aton SJ (2017). Parvalbumin-expressing interneurons coordinate hippocampal network dynamics required for memory consolidation. Nature communications 8, 15039. 10.1038/ncomms15039.
64. Schneider P, Bayo-Fina JM, Singh R, Kumar Dhanyamraju P, Holz P, Baier A, Fendrich V, Ramaswamy A, Baumeister S, Martinez ED, and Lauth M (2015). Identification of a novel actin-dependent signal transducing module allows for the targeted degradation of GLI1. Nature communications 6, 8023. 10.1038/ncomms9023.
65. Singh R, and Lauth M (2017). Emerging Roles of DYRK Kinases in Embryogenesis and Hedgehog Pathway Control. J Dev Biol 5. 10.3390/jdb5040013.
66. De Toma I, Ortega M, Aloy P, Sabido E, and Dierssen M (2019). DYRK1A Overexpression Alters Cognition and Neural-Related Proteomic Pathways in the Hippocampus That Are Rescued by Green Tea Extract and/or Environmental Enrichment. Front Mol Neurosci 12, 272. 10.3389/fnmol.2019.00272. [PubMed: 31803016]
67. Barrientos T, Frank D, Kuwahara K, Bezprozvannaya S, Pipes GC, Bassel-Duby R, Richardson JA, Katus HA, Olson EN, and Frey N (2007). Two novel members of the ABLIM protein family, ABLIM-2 and -3, associate with STARS and directly bind F-actin. J Biol Chem 282, 8393–8403. 10.1074/jbc.M607549200. [PubMed: 17194709]

68. Cao J, Shen Y, Zhu L, Xu Y, Zhou Y, Wu Z, Li Y, Yan X, and Zhu X (2012). miR-129-3p controls cilia assembly by regulating CP110 and actin dynamics. Nature cell biology 14, 697–706. 10.1038/ncb2512. [PubMed: 22684256]
69. Yang S, Liu C, Guo Y, Li G, Li D, Yan X, and Zhu X (2022). Self-construction of actin networks through phase separation-induced abLIM1 condensates. Proc Natl Acad Sci U S A 119, e2122420119. 10.1073/pnas.2122420119. [PubMed: 35858327]
70. Li G, Huang S, Yang S, Wang J, Cao J, Czajkowsky DM, Shao Z, and Zhu X (2018). abLIM1 constructs non-erythroid cortical actin networks to prevent mechanical tension-induced blebbing. Cell Discov 4, 42. 10.1038/s41421-018-0040-3. [PubMed: 30062045]
71. Grintsevich EE, Ahmed G, Ginosyan AA, Wu H, Rich SK, Reisler E, and Terman JR (2021). Profilin and Mical combine to impair F-actin assembly and promote disassembly and remodeling. Nature communications 12, 5542. 10.1038/s41467-021-25781-3.
72. Rizzardi LF, Hickey PF, Idrizi A, Tryggvadottir R, Callahan CM, Stephens KE, Taverna SD, Zhang H, Ramazanoglu S, Consortium GT, et al. (2021). Human brain region-specific variably methylated regions are enriched for heritability of distinct neuropsychiatric traits. Genome biology 22, 116. 10.1186/s13059-021-02335-w. [PubMed: 33888138]
73. Rollenhagen A, and Lubke JH (2010). The mossy fiber bouton: the "common" or the "unique" synapse? Front Synaptic Neurosci 2, 2. 10.3389/fnsyn.2010.00002. [PubMed: 21423488]
74. Heffner CS, Herbert Pratt C, Babiuk RP, Sharma Y, Rockwood SF, Donahue LR, Eppig JT, and Murray SA (2012). Supporting conditional mouse mutagenesis with a comprehensive cre characterization resource. Nature communications 3, 1218. 10.1038/ncomms2186.
75. Lakso M, Pichel JG, Gorman JR, Sauer B, Okamoto Y, Lee E, Alt FW, and Westphal H (1996). Efficient in vivo manipulation of mouse genomic sequences at the zygote stage. Proc Natl Acad Sci U S A 93, 5860–5865. 10.1073/pnas.93.12.5860. [PubMed: 8650183]
76. Guo D, Peng Y, Wang L, Sun X, Wang X, Liang C, Yang X, Li S, Xu J, Ye WC, et al. (2021). Autism-like social deficit generated by Dock4 deficiency is rescued by restoration of Rac1 activity and NMDA receptor function. Mol Psychiatry 26, 1505–1519. 10.1038/s41380-019-0472-7. [PubMed: 31388105]
77. Holzenberger M, Lenzner C, Leneuve P, Zaoui R, Hamard G, Vaulont S, and Bouc YL (2000). Cre-mediated germline mosaicism: a method allowing rapid generation of several alleles of a target gene. Nucleic Acids Res 28, E92. 10.1093/nar/28.21.e92. [PubMed: 11058142]
78. Madisen L, Zwingman TA, Sunkin SM, Oh SW, Zariwala HA, Gu H, Ng LL, Palmiter RD, Hawrylycz MJ, Jones AR, et al. (2010). A robust and high-throughput Cre reporting and characterization system for the whole mouse brain. Nat Neurosci 13, 133–140. 10.1038/nn.2467. [PubMed: 20023653]
79. Woods YL, Rena G, Morrice N, Barthel A, Becker W, Guo S, Unterman TG, and Cohen P (2001). The kinase DYRK1A phosphorylates the transcription factor FKHR at Ser329 in vitro, a novel in vivo phosphorylation site. Biochem J 355, 597–607. 10.1042/bj3550597. [PubMed: 11311120]
80. Guo X, Williams JG, Schug TT, and Li X (2010). DYRK1A and DYRK3 promote cell survival through phosphorylation and activation of SIRT1. J Biol Chem 285, 13223–13232. 10.1074/jbc.M110.102574. [PubMed: 20167603]
81. Himpel S, Tegge W, Frank R, Leder S, Joost HG, and Becker W (2000). Specificity determinants of substrate recognition by the protein kinase DYRK1A. J Biol Chem 275, 2431–2438. 10.1074/jbc.275.4.2431. [PubMed: 10644696]
82. Vormstein-Schneider D, Lin JD, Pelkey KA, Chittajallu R, Guo B, Arias-Garcia MA, Allaway K, Sakopoulos S, Schneider G, Stevenson O, et al. (2020). Viral manipulation of functionally distinct interneurons in mice, non-human primates and humans. Nat Neurosci 23, 1629–1636. 10.1038/s41593-020-0692-9. [PubMed: 32807948]
83. Conti LR (2021). Karl Deisseroth, Peter Hegemann, and Dieter Oesterhelt receive the 2021 Albert Lasker Basic Medical Research Award. J Clin Invest 131. 10.1172/JCI154418.
84. Roth BL (2016). DREADDs for Neuroscientists. Neuron 89, 683–694. 10.1016/j.neuron.2016.01.040. [PubMed: 26889809]
85. Fotaki V, Dierssen M, Alcantara S, Martinez S, Marti E, Casas C, Visa J, Soriano E, Estivill X, and Arbones ML (2002). Dyrk1A haploinsufficiency affects viability and causes

developmental delay and abnormal brain morphology in mice. Mol Cell Biol 22, 6636–6647. 10.1128/MCB.22.18.6636-6647.2002. [PubMed: 12192061]

86. Raveau M, Shimohata A, Amano K, Miyamoto H, and Yamakawa K (2018). DYRK1A-haploinsufficiency in mice causes autistic-like features and febrile seizures. Neurobiol Dis 110, 180–191. 10.1016/j.nbd.2017.12.003. [PubMed: 29223763]
87. Chattopadhyaya B, Di Cristo G, Higashiyama H, Knott GW, Kuhlman SJ, Welker E, and Huang ZJ (2004). Experience and activity-dependent maturation of perisomatic GABAergic innervation in primary visual cortex during a postnatal critical period. J Neurosci 24, 9598–9611. 10.1523/JNEUROSCI.1851-04.2004. [PubMed: 15509747]
88. McFarlan AR, Chou CYC, Watanabe A, Cherepacha N, Haddad M, Owens H, and Sjostrom PJ (2023). The plasticitome of cortical interneurons. Nat Rev Neurosci 24, 80–97. 10.1038/s41583-022-00663-9. [PubMed: 36585520]
89. Modol L, Bollmann Y, Tressard T, Baude A, Che A, Duan ZRS, Babij R, De Marco Garcia NV, and Cossart R (2020). Assemblies of Perisomatic GABAergic Neurons in the Developing Barrel Cortex. Neuron 105, 93–105 e104. 10.1016/j.neuron.2019.10.007. [PubMed: 31780328]
90. Campanac E, Gasselin C, Baude A, Rama S, Ankri N, and Debanne D (2013). Enhanced intrinsic excitability in basket cells maintains excitatory-inhibitory balance in hippocampal circuits. Neuron 77, 712–722. 10.1016/j.neuron.2012.12.020. [PubMed: 23439123]
91. Li KX, Lu YM, Xu ZH, Zhang J, Zhu JM, Zhang JM, Cao SX, Chen XJ, Chen Z, Luo JH, et al. (2011). Neuregulin 1 regulates excitability of fast-spiking neurons through Kv1.1 and acts in epilepsy. Nat Neurosci 15, 267–273. 10.1038/nn.3006. [PubMed: 22158511]
92. Dehorter N, Ciceri G, Bartolini G, Lim L, del Pino I, and Marin O (2015). Tuning of fast-spiking interneuron properties by an activity-dependent transcriptional switch. Science 349, 1216–1220. 10.1126/science.aab3415. [PubMed: 26359400]
93. Exposito-Alonso D, and Rico B (2022). Mechanisms Underlying Circuit Dysfunction in Neurodevelopmental Disorders. Annu Rev Genet 56, 391–422. 10.1146/annurev-genet-072820-023642. [PubMed: 36055969]
94. Favuzzi E, Deogracias R, Marques-Smith A, Maeso P, Jezequel J, Exposito-Alonso D, Balia M, Kroon T, Hinojosa AJ, F.M. E, and Rico B (2019). Distinct molecular programs regulate synapse specificity in cortical inhibitory circuits. Science 363, 413–417. 10.1126/science.aau8977. [PubMed: 30679375]
95. Uezu A, Kanak DJ, Bradshaw TW, Soderblom EJ, Catavero CM, Burette AC, Weinberg RJ, and Soderling SH (2016). Identification of an elaborate complex mediating postsynaptic inhibition. Science 353, 1123–1129. 10.1126/science.aag0821. [PubMed: 27609886]
96. Allaway KC, Gabitto MI, Wapinski O, Saldi G, Wang CY, Bandler RC, Wu SJ, Bonneau R, and Fishell G (2021). Genetic and epigenetic coordination of cortical interneuron development. Nature 597, 693–697. 10.1038/s41586-021-03933-1. [PubMed: 34552240]
97. Bernard C, Exposito-Alonso D, Selten M, Sanalidou S, Hanusz-Godoy A, Aguilera A, Hamid F, Oozeer F, Maeso P, Allison L, et al. (2022). Cortical wiring by synapse type-specific control of local protein synthesis. Science 378, eabm7466. 10.1126/science.abm7466. [PubMed: 36423280]
98. Chiang MC, Huang AJY, Wintzer ME, Ohshima T, and McHugh TJ (2018). A role for CA3 in social recognition memory. Behav Brain Res 354, 22–30. 10.1016/j.bbr.2018.01.019. [PubMed: 29355673]
99. Leung C, Cao F, Nguyen R, Joshi K, Aqrabawi AJ, Xia S, Cortez MA, Snead OC 3rd, Kim JC, and Jia Z (2018). Activation of Entorhinal Cortical Projections to the Dentate Gyrus Underlies Social Memory Retrieval. Cell reports 23, 2379–2391. 10.1016/j.celrep.2018.04.073. [PubMed: 29791849]
100. Li J, Sun X, You Y, Li Q, Wei C, Zhao L, Sun M, Meng H, Zhang T, Yue W, et al. (2022). Auts2 deletion involves in DG hypoplasia and social recognition deficit: The developmental and neural circuit mechanisms. Sci Adv 8, eabk1238. 10.1126/sciadv.abk1238. [PubMed: 35235353]
101. Cope EC, Waters RC, Diethorn EJ, Pagliai KA, Dias CG, Tsuda M, Cameron HA, and Gould E (2020). Adult-Born Neurons in the Hippocampus Are Essential for Social Memory Maintenance. eNeuro 7. 10.1523/ENEURO.0182-20.2020.

102. Oliva A (2022). Neuronal ensemble dynamics in social memory. Curr Opin Neurobiol 78, 102654. 10.1016/j.conb.2022.102654. [PubMed: 36509026]
103. Deng X, Gu L, Sui N, Guo J, and Liang J (2019). Parvalbumin interneuron in the ventral hippocampus functions as a discriminator in social memory. Proc Natl Acad Sci U S A 116, 16583–16592. 10.1073/pnas.1819133116. [PubMed: 31358646]
104. Gómez-Ocádiz R, Trippa M, Posani L, Cocco S, Monasson R, and Schmidt-Hieber C (2021). A synaptic novelty signal to switch hippocampal attractor networks from generalization to discrimination. bioRxiv, 2021.2002.2024.432612. 10.1101/2021.02.24.432612.
105. Sasaki T, Piatti VC, Hwaun E, Ahmadi S, Lisman JE, Leutgeb S, and Leutgeb JK (2018). Dentate network activity is necessary for spatial working memory by supporting CA3 sharp-wave ripple generation and prospective firing of CA3 neurons. Nat Neurosci 21, 258–269. 10.1038/s41593-017-0061-5. [PubMed: 29335604]
106. Vancura B, Geiller T, Grosmark A, Zhao V, and Losonczy A (2023). Inhibitory control of sharp-wave ripple duration during learning in hippocampal recurrent networks. Nat Neurosci 26, 788–797. 10.1038/s41593-023-01306-7. [PubMed: 37081295]
107. Sadeh S, and Clopath C (2021). Inhibitory stabilization and cortical computation. Nat Rev Neurosci 22, 21–37. 10.1038/s41583-020-00390-z. [PubMed: 33177630]
108. Boehringer R, Polygalov D, Huang AJY, Middleton SJ, Robert V, Wintzer ME, Piskorowski RA, Chevaleyre V, and McHugh TJ (2017). Chronic Loss of CA2 Transmission Leads to Hippocampal Hyperexcitability. Neuron 94, 642–655 e649. 10.1016/j.neuron.2017.04.014. [PubMed: 28472661]
109. Nasrallah K, Therreau L, Robert V, Huang AJY, McHugh TJ, Piskorowski RA, and Chevaleyre V (2019). Routing Hippocampal Information Flow through Parvalbumin Interneuron Plasticity in Area CA2. Cell reports 27, 86–98 e83. 10.1016/j.celrep.2019.03.014. [PubMed: 30943417]
110. Fernandez-Lamo I, Gomez-Dominguez D, Sanchez-Aguilera A, Oliva A, Morales AV, Valero M, Cid E, Berenyi A, and Menendez de la Prida L (2019). Proximodistal Organization of the CA2 Hippocampal Area. Cell reports 26, 1734–1746 e1736. 10.1016/j.celrep.2019.01.060. [PubMed: 30759386]
111. Middleton SJ, and McHugh TJ (2020). CA2: A Highly Connected Intrahippocampal Relay. Annu Rev Neurosci 43, 55–72. 10.1146/annurev-neuro-080719-100343. [PubMed: 31874067]
112. Stober TM, Lehr AB, Hafting T, Kumar A, and Fyhn M (2020). Selective neuromodulation and mutual inhibition within the CA3-CA2 system can prioritize sequences for replay. Hippocampus 30, 1228–1238. 10.1002/hipo.23256. [PubMed: 32870537]
113. Robert V, Therreau L, Chevaleyre V, Lepicard E, Viollet C, Cognet J, Huang AJ, Boehringer R, Polygalov D, McHugh TJ, and Piskorowski RA (2021). Local circuit allowing hypothalamic control of hippocampal area CA2 activity and consequences for CA1. eLife 10. 10.7554/eLife.63352.
114. Wu X, Morishita W, Beier KT, Heifets BD, and Malenka RC (2021). 5-HT modulation of a medial septal circuit tunes social memory stability. Nature 599, 96–101. 10.1038/s41586-021-03956-8. [PubMed: 34616037]
115. Lee YH, Im E, Hyun M, Park J, and Chung KC (2021). Protein phosphatase PPM1B inhibits DYRK1A kinase through dephosphorylation of pS258 and reduces toxic tau aggregation. J Biol Chem 296, 100245. 10.1074/jbc.RA120.015574. [PubMed: 33380426]
116. Ruiz-Mejias M, Martinez de Lagran M, Mattia M, Castano-Prat P, Perez-Mendez L, Ciria-Suarez L, Gener T, Sancristobal B, Garcia-Ojalvo J, Gruart A, et al. (2016). Overexpression of Dyrk1A, a Down Syndrome Candidate, Decreases Excitability and Impairs Gamma Oscillations in the Prefrontal Cortex. J Neurosci 36, 3648–3659. 10.1523/JNEUROSCI.2517-15.2016. [PubMed: 27030752]
117. Guy J, Gan J, Selfridge J, Cobb S, and Bird A (2007). Reversal of neurological defects in a mouse model of Rett syndrome. Science 315, 1143–1147. 10.1126/science.1138389. [PubMed: 17289941]
118. Ehninger D, Li W, Fox K, Stryker MP, and Silva AJ (2008). Reversing neurodevelopmental disorders in adults. Neuron 60, 950–960. S0896-6273(08)01055-6 [pii] 10.1016/j.neuron.2008.12.007. [PubMed: 19109903]

119. Mielnik CA, Binko MA, Chen Y, Funk AJ, Johansson EM, Intson K, Sivananthan N, Islam R, Milenkovic M, Horsfall W, et al. (2021). Consequences of NMDA receptor deficiency can be rescued in the adult brain. Mol Psychiatry 26, 2929–2942. 10.1038/s41380-020-00859-4. [PubMed: 32807843]
120. Sztainberg Y, Chen HM, Swann JW, Hao S, Tang B, Wu Z, Tang J, Wan YW, Liu Z, Rigo F, and Zoghbi HY (2015). Reversal of phenotypes in MECP2 duplication mice using genetic rescue or antisense oligonucleotides. Nature 528, 123–126. 10.1038/nature16159. [PubMed: 26605526]
121. Davidson BL, Gao G, Berry-Kravis E, Bradbury AM, Bonnemann C, Buxbaum JD, Corcoran GR, Gray SJ, Gray-Edwards H, Kleiman RJ, et al. (2022). Gene-based therapeutics for rare genetic neurodevelopmental psychiatric disorders. Molecular therapy : the journal of the American Society of Gene Therapy 30, 2416–2428. 10.1016/j.ymthe.2022.05.014. [PubMed: 35585789]
122. Sun J, and Roy S (2021). Gene-based therapies for neurodegenerative diseases. Nat Neurosci 24, 297–311. 10.1038/s41593-020-00778-1. [PubMed: 33526943]
123. Segel M, Lash B, Song J, Ladha A, Liu CC, Jin X, Mekhedov SL, Macrae RK, Koonin EV, and Zhang F (2021). Mammalian retrovirus-like protein PEG10 packages its own mRNA and can be pseudotyped for mRNA delivery. Science 373, 882–889. 10.1126/science.abg6155. [PubMed: 34413232]
124. Dunbar CE, High KA, Joung JK, Kohn DB, Ozawa K, and Sadelain M (2018). Gene therapy comes of age. Science 359. 10.1126/science.aan4672.
125. Nagata T, Dwyer CA, Yoshida-Tanaka K, Ihara K, Ohyagi M, Kaburagi H, Miyata H, Ebihara S, Yoshioka K, Ishii T, et al. (2021). Cholesterol-functionalized DNA/RNA heteroduplexes cross the blood-brain barrier and knock down genes in the rodent CNS. Nature biotechnology. 10.1038/s41587-021-00972-x.
126. Roberts TC, Langer R, and Wood MJA (2020). Advances in oligonucleotide drug delivery. Nature reviews. Drug discovery 19, 673–694. 10.1038/s41573-020-0075-7. [PubMed: 32782413]
127. Goertsen D, Flytzanis NC, Goeden N, Chuapoco MR, Cummins A, Chen Y, Fan Y, Zhang Q, Sharma J, Duan Y, et al. (2021). AAV capsid variants with brain-wide transgene expression and decreased liver targeting after intravenous delivery in mouse and marmoset. Nat Neurosci. 10.1038/s41593-021-00969-4.
128. McCauley ME, and Bennett CF (2023). Antisense drugs for rare and ultra-rare genetic neurological diseases. Neuron 111, 2465–2468. 10.1016/j.neuron.2023.05.027. [PubMed: 37354903]
129. Han SP, Scherer L, Gethers M, Salvador AM, Salah MBH, Mancusi R, Sagar S, Hu R, DeRogatis J, Kuo YH, et al. (2022). Programmable siRNA pro-drugs that activate RNAi activity in response to specific cellular RNA biomarkers. Mol Ther Nucleic Acids 27, 797–809. 10.1016/j.omtn.2021.12.039. [PubMed: 35116191]
130. Martin EA, Muralidhar S, Wang Z, Cervantes DC, Basu R, Taylor MR, Hunter J, Cutforth T, Wilke SA, Ghosh A, and Williams ME (2015). The intellectual disability gene Kirrel3 regulates target-specific mossy fiber synapse development in the hippocampus. eLife 4. 10.7554/eLife.09395.
131. Wang X, Spandidos A, Wang H, and Seed B (2012). PrimerBank: a PCR primer database for quantitative gene expression analysis, 2012 update. Nucleic Acids Res 40, D1144–1149. 10.1093/nar/gkr1013. [PubMed: 22086960]
132. Hanes AL, Koesters AG, Fong MF, Altimimi HF, Stellwagen D, Wenner P, and Engisch KL (2020). Divergent Synaptic Scaling of Miniature EPSCs following Activity Blockade in Dissociated Neuronal Cultures. J Neurosci 40, 4090–4102. 10.1523/JNEUROSCI.1393-19.2020. [PubMed: 32312887]
133. Landis SC, Amara SG, Asadullah K, Austin CP, Blumenstein R, Bradley EW, Crystal RG, Darnell RB, Ferrante RJ, Fillit H, et al. (2012). A call for transparent reporting to optimize the predictive value of preclinical research. Nature 490, 187–191. 10.1038/nature11556. [PubMed: 23060188]
134. Kilkenny C, Browne WJ, Cuthill IC, Emerson M, and Altman DG (2010). Improving bioscience research reporting: the ARRIVE guidelines for reporting animal research. PLoS Biol 8, e1000412. 10.1371/journal.pbio.1000412. [PubMed: 20613859]

Highlights

DYRK1A in mossy fibers recruits PV IN mediated feed-forward inhibition of CA3 and CA2 DYRK1A-ABLIM3 signaling in mossy fiber-PV IN synapses promotes inhibition of CA3 and CA2 *Ablim3* downregulation in *Dyrk1a*$^{+/-}$ mice rescues PV IN and social recognition deficits Chemogenetic activation of PV INs in CA3/CA2 rescues social recognition in *Dyrk1a*$^{+/-}$ mice

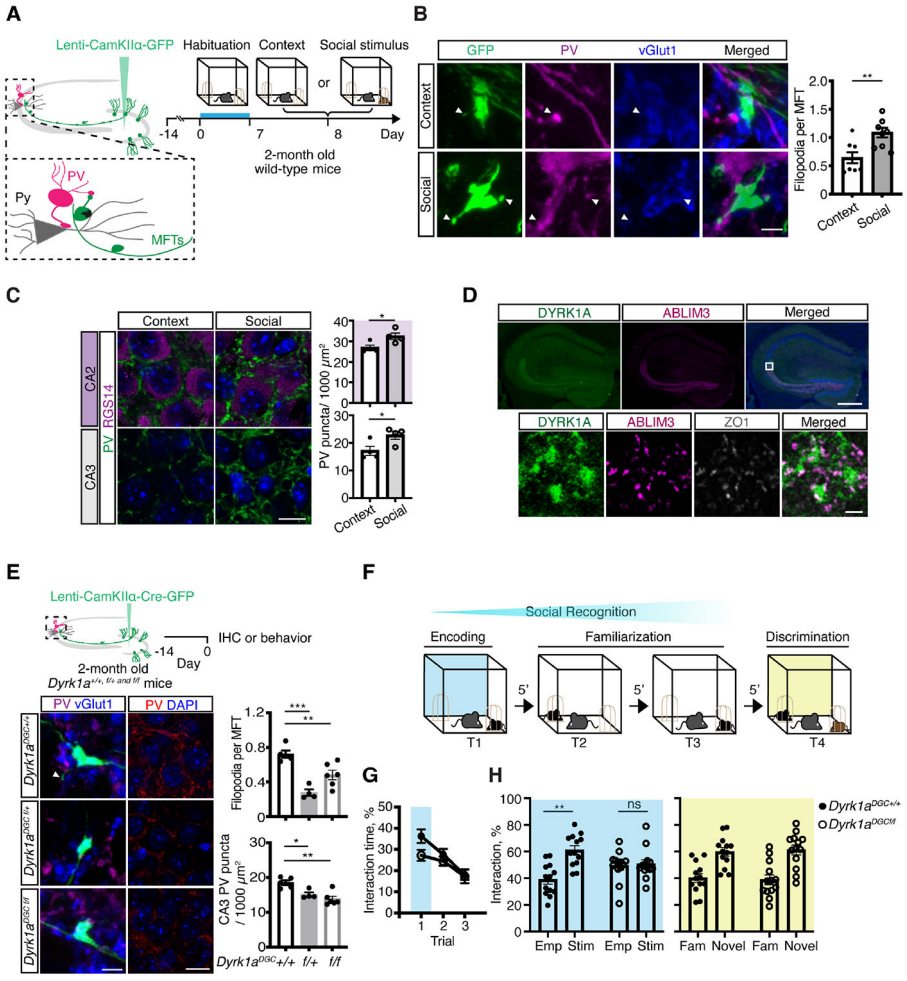

Figure 1. *Dyrk1a* is required in DGCs of adult mice for FFI connectivity, PV IN perisomatic contacts and social recognition

(A) Experimental design. Lentiviruses expressing GFP (CaMKIIα-GFP) were injected into the DG of 2-month old WT mice 2 weeks prior to habituation to a chamber (Context) for 7 days. On day 8 mice were exposed to the familiarized context or familiarized context with a social stimulus (novel juvenile mouse).

(B) Representative images showing GFP$^+$ MFTs (filopodial extensions, arrows) and quantification of the number of filopodia per vGLUT1$^+$ MFTs (N = 8 mice per group). Scale bar, 5 μm. $^{**}p$; < 0.01 using two-tailed unpaired *t* test with Welch's correction.

(C) Representative images and quantification of PV$^+$ puncta density in CA2/CA3 stratum pyramidale (N =4 mice per group). Top, RGS14$^+$ labeling defines CA2 subfield. Scale bar, 10 μm. $^*p < 0.05$ using two-tailed unpaired *t* test with Welch's correction

(D) Images showing co-immunostaining of DYRK1A, ABLIM3 and ZO1 in hippocampus. Scale bar, 100 μm. Inset shows high magnification of dorsal CA3 subregion outlined in image. Scale bar, 5 μm.

(E) Lentiviruses expressing CaMKIIα-Cre-T2A-GFP were injected into DG of 2-month old *Dyrk1a*$^{f/f,\ f/+\ and\ +/+}$ mice 2 weeks prior to processing for morphology analysis or use in social cognition behavioral paradigm. Representative images showing GFP$^+$ MFTs

(filopodia extensions, arrows) and quantification of the number of vGLUT1$^+$ filopodia per MFT in CA3 (left) and PV$^+$ puncta density in CA3 (right)(N = 5 for mice +/+; 4 mice for *f/+*; 6 mice for *f/f*). Scale bar, 5 μm (left); 10 μm (right). $^{**}p < 0.01$; $^{***}p < 0.001$ using one-way ANOVA with Bonferroni post hoc test.

(F) Schematic of social cognition task depicting social recognition (encoding: trial1, T1 and two trials of familiarization to social stimulus, T2-T3) and social memory discrimination trial (T4), each trial separated by 5 min intervals.

(G) Quantification of total interaction time during T1-T3. Blue shaded box outlines social recognition phase (T1).

(H) Quantification of empty cup vs. social stimulus interaction time during social recognition phase (T1) (left panel, blue shaded) and the discrimination trial (T4, right panel, yellow shaded) (N =13 mice per group). Emp, empty pencil cup; stim, stimulus mouse; fam, familiar mouse; novel, a new novel stimulus mouse. $^{**}p < 0.01$ using two-way ANOVA with Bonferroni post hoc test.

All experiments are performed in male mice and all data are displayed as mean ± SEM. See also Figure S1.

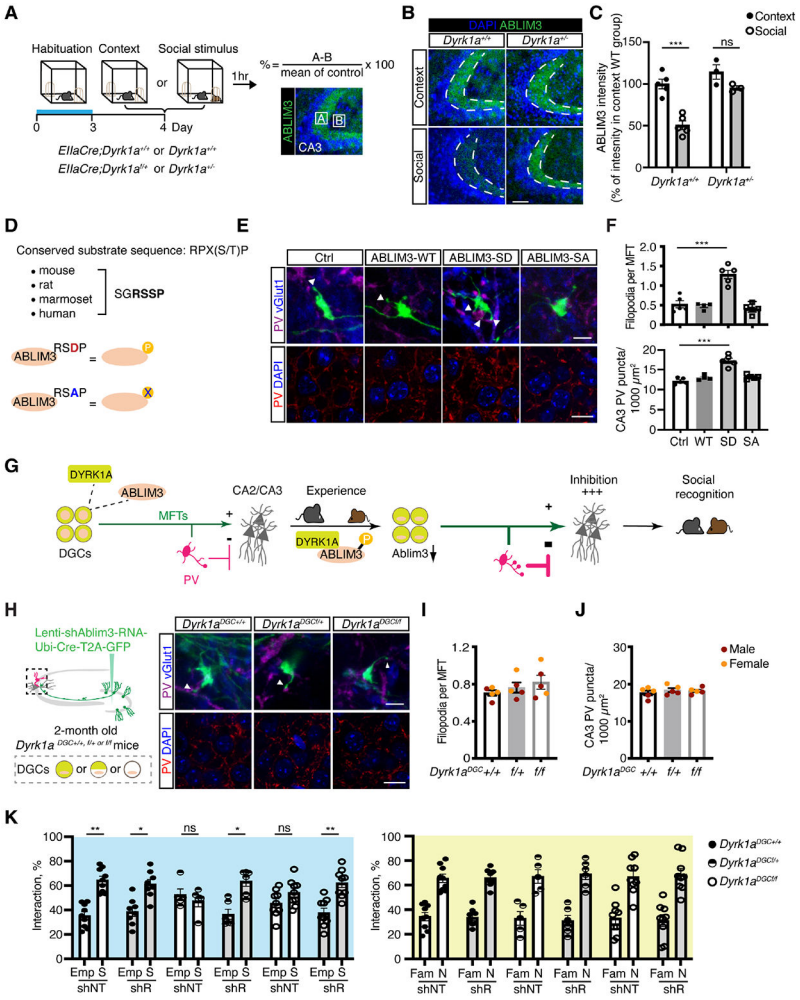

Figure 2. ABLIM3 functions downstream of DYRK1A in mossy fibers to regulate FFI connectivity, PV IN perisomatic contacts and social recognition

(A) Schematic of experimental design and quantification of ABLIM3 levels in mossy fiber terminals in *EIIaCre;Dyrk1a*$^{+/+\ or\ f/+}$ mice (referred to as *Dyrk1a*$^{+/+\ or\ +/-}$).

(B) Representative images of ABLIM3 immunoreactivity in mossy fiber terminals in *Dyrk1a*$^{+/+\ or\ +/-}$ mice. Dashed lines indicate ABLIM3 in mossy fibers. Scale bar, 100 μm.

(C) Quantification of ABLIM3 levels in mossy fiber terminals (MFTs) in 2-3 month old mice (In *Dyrk1a*$^{+/+}$, N = 5 mice for each group; in *Dyrk1a*$^{+/-}$, N = 3 mice for each group). $^{**}p < 0.01$ using two-way ANOVA with Bonferroni post hoc test.

(D) Conserved DYRK1A phosphorylation site in ABLIM3 based on consensus sequence.

(E-F) Representative images of MFTs and PV puncta taken from mice following lentiviral overexpression of GFP (Ctrl), ABLIM3 wild-type (WT), phosphomimetic ABLIM3 (SD) or phospho-dead ABLIM3 (SA) mutants in DG of 2-month old WT mice. Representative images and quantification of number of filopodia per vGLUT1^{+} MFT in CA3 (top) and PV^{+} puncta density in CA3 (bottom). Scale bar, 5 μm (top); 10 μm (bottom). (N = 5 mice for vector control; 4 mice for WT; 5 mice for SD; 5 mice for SA). $^{***}p < 0.001$ using one-way ANOVA with Bonferroni post hoc test.

(G) Working model for how DYRK1A-dependent ABLIM3 phosphorylation in MFTs recruits PV mediated perisomatic inhibition in CA3/CA2. Yellow color denotes DYRK1A levels and peach color denotes ABLIM3 levels in DGCs and mossy fibers.
(H) Schematic of lentivirus injection of U6-*Ablim3* shRNA-Ubi-Cre-T2A-GFP-cassette into DG of 2-month old *Dyrk1a*$^{+/+,\ f/+\ or\ f/f}$ mice. Representative images showing GFP$^+$ MFTs (filopodia extensions, arrows, top) PV$^+$ puncta density in CA3 (bottom). Scale bar, 5 μm (top); 10 μm (bottom).
(I-J) Quantification of the number of vGLUT1$^+$ filopodia per MFT (H) and PV$^+$ puncta density (I) in CA3 stratum pyramidale (N = 5 mice for each group). $p > 0.05$ using one-way ANOVA with Bonferroni post hoc test.
(K) Quantification of interaction time during social recognition phase (T1, left panel, blue shaded) and social memory discrimination phase (T4, right panel, yellow shaded). 2-month old mice injected with shNT (N = 9 mice for +/+; 5 mice for *f/+*; 9 mice for *f/f* mice) or shRNA (N = 8 mice for *+/+*; 6 mice for *f/+*; 9 mice for *f/f* mice). Emp, empty pencil cup; stim, stimulus mouse; fam, familiar mouse; novel, a new novel stimulus mouse. *$p < 0.05$; **$p < 0.01$ using two-way ANOVA with Bonferroni post hoc test.
These experiments are performed in male mice (C, F, K) or male and female (I-J).
All data are displayed as mean ± SEM.
See also Figure S2-S4.

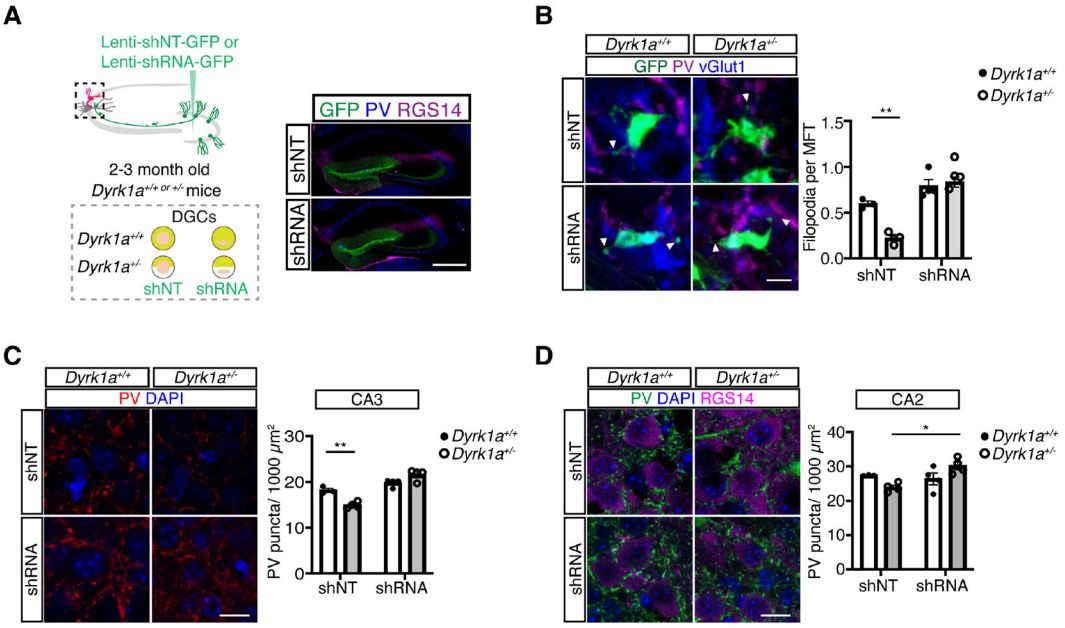

Figure 3. *Ablim3* downregulation in DGCs of adult heterozygous *Dyrk1a* mice restores FFI connectivity and PV IN perisomatic contacts in CA3 and CA2

(A) Lentiviruses expressing *Ablim3* shRNA-GFP or non-targeting shRNA (shNT-GFP) were injected into DG of 2-3 month old *Dyrk1a*$^{+/+ \text{ or } +/-}$ mice. Representative images showing viral expression of GFP in DG and RGS14 immunostaining to delineate CA2. Scale bar, 500 μm.

(B) Representative images showing GFP+ MFTs and quantification of the number of vGLUT1^{+} filopodia per MFT (in *Dyrk1a*$^{+/+}$, N = 3 mice for shNT; N=4 mice for shRNA; in *Dyrk1a*$^{+/-}$, N=4 mice for each group) in CA3. Scale bar, 5 μm. $^{**}p < 0.01$ using two-way ANOVA with Bonferroni post hoc test.

(C-D) Representative images and quantification of PV^{+} puncta density in CA3 (C) and CA2 (D) subfields. Scale bar, 10 μm. *p < 0.05; **p < 0.01 using two-way ANOVA with Bonferroni post hoc test.

These experiments are performed in male mice.

All data are displayed as mean ± SEM. See also Figure S5.

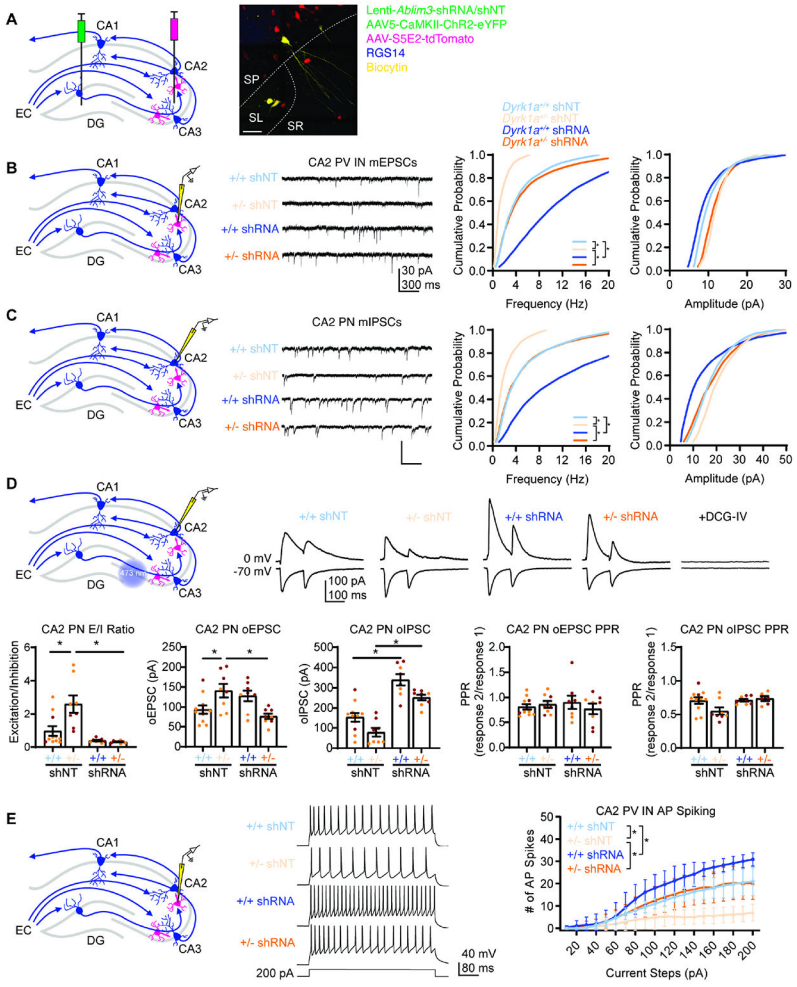

Figure 4. *Ablim3* downregulation in DGCs of adult heterozygous *Dyrk1a* mice restores inhibitory synaptic transmission in DG-CA2

(A) Schematic depicting lentiviral-*Ablim3*-shRNA/shNT and rAAV5-CaMKIIα-ChR2-eYFP injection into DG, and AAV-S5E2-tdTomato injected into CA3/CA2 (left). Representative image of CA2 showing eYFP expression in MFTs in stratum lucidum (SL), tdTomato expressed in PV INs, RGS14 immunostaining of CA2, and immunostaining of biocytin-filled PN and PV INs. Scale bar, 50 μm.

(B) Schematic depicting whole-cell patch-clamp recording of miniature excitatory postsynaptic current (mEPSC) from CA2 PV IN (left). Representative recording traces from each group (middle). Cumulative probability plots of mEPSC frequency and amplitude from PV INs (Kolmogorov-Smirnov test, $*p < 0.05$, n=8-9 cells, 2-3 cells per mouse, 3-4 mice per group).

(C) Schematic depicting whole-cell patch-clamp recording of miniature inhibitory postsynaptic current (mIPSC) from CA2 pyramidal neurons (PN) (left). Representative traces from each group (middle). Cumulative probability plots of mIPSC frequency and amplitude from PNs (Kolmogorov-Smirnov test, $*p < 0.05$, n=8-9 cells, 2-3 cells per mouse, 3-4 mice per group).

(D) Schematic depicting whole-cell patch-clamp recording of EPSC and IPSC from CA2 PN to paired pulse optical (473 nm) stimulation. Representative traces from each group and traces after perfusion of DCG-IV. Bar graphs indicate excitation to inhibition ratio, the amplitude of the first EPSC and IPSC response to paired pulse optical stimulation, and the EPSC and IPSC paired pulse ratios. (Two-way ANOVA with Tukey posthoc, $*p < 0.05$, n=8-11 cells, 2-3 cells per mouse, 3-4 mice per group).

(E) Schematic depicting whole-cell patch-clamp recording of CA2 PV IN in current-clamp configuration.

Representative traces from each group depict action potential response to current steps (200 pA, 500 ms). Line graph indicates number of potential responses to incremental current steps (Two-way RM ANOVA with Tukey posthoc, $*p < 0.05$, n=11-12 cells, 2-3 cells per mouse, 5-6 mice per group).

All data are displayed as mean ± SEM.

These experiments are performed in male and female mice.

See also Figure S6.

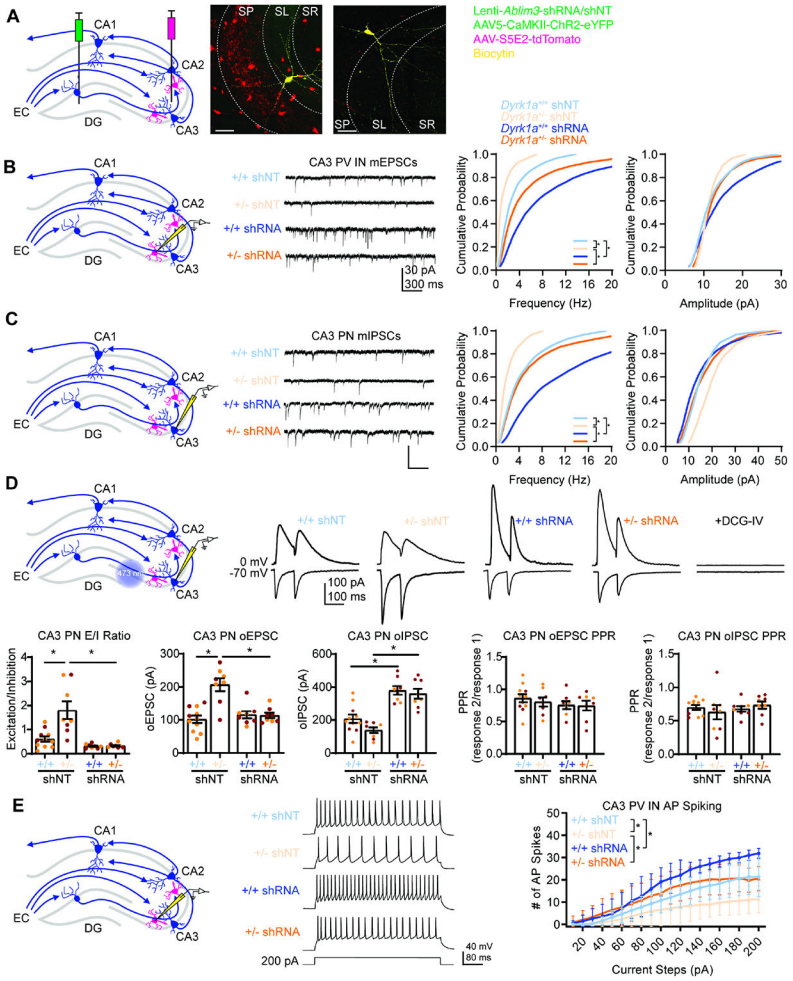

Figure 5. *Ablim3* downregulation in DGCs of adult heterozygous *Dyrk1a* mice restores inhibitory synaptic transmission in DG-CA3

(A) Schematic depicting lentiviral-*Ablim3*-shRNA/shNT and rAAV$_5$-CaMKIIα-ChR2-eYFP injection into DG, and AAV-S5E2-tdTomato injected into CA3/CA2 (left). Representative image of CA2 showing eYFP expression in MFTs in the stratum lucidum (SL), tdTomato expressed in PV$^+$ INs, and immunostaining of biocytin-filled PN and PV$^+$ INs. Scale bar, 50 μm.

(B) Schematic depicting whole-cell patch-clamp recording of mEPSC from CA3 PV IN (left). Representative recording traces from each group (middle). Cumulative probability plots of mEPSC frequency and amplitude from PV INs (Kolmogorov-Smirnov test, *$p <$ 0.05, n=8-9 cells, 2-3 cells per mouse, 3-4 mice per group).

(C) Schematic depicting whole-cell patch-clamp recording of mIPSC from CA3 PN (left). Representative traces from each group (middle). Cumulative probability plots of mIPSC frequency and amplitude from PNs (Kolmogorov-Smirnov test, *$p < 0.05$, n=8-9 cells, 2-3 cells per mouse, 3-4 mice per group).

(D) Schematic depicting whole-cell patch-clamp recording of EPSC and IPSC from CA3 PN to paired pulse optical (473 nm) stimulation. Representative traces from each group and traces after perfusion of DCG-IV. Bar graphs indicate excitation to inhibition ratio, the

amplitude of the first EPSC and IPSC response to paired pulse optical stimulation, and the EPSC and IPSC paired pulse ratios. (Two-way ANOVA with Tukey posthoc, $*p < 0.05$, n=8-11 cells, 2-3 cells per mouse, 3-4 mice per group).

(E) Schematic depicting whole-cell patch-clamp recording of CA3 PV^+ IN in current-clamp configuration. Representative traces from each group depict action potential response to current steps (200 pA, 500 ms). Line graph indicates number of potential responses to incremental current steps (Two-way RM ANOVA with Tukey posthoc, $*p < 0.05$, n=13-13 cells, 2-3 cells per mouse, 5-7 mice per group).

All data are displayed as mean ± SEM.

These experiments are performed in male and female mice.

See also Figure S7.

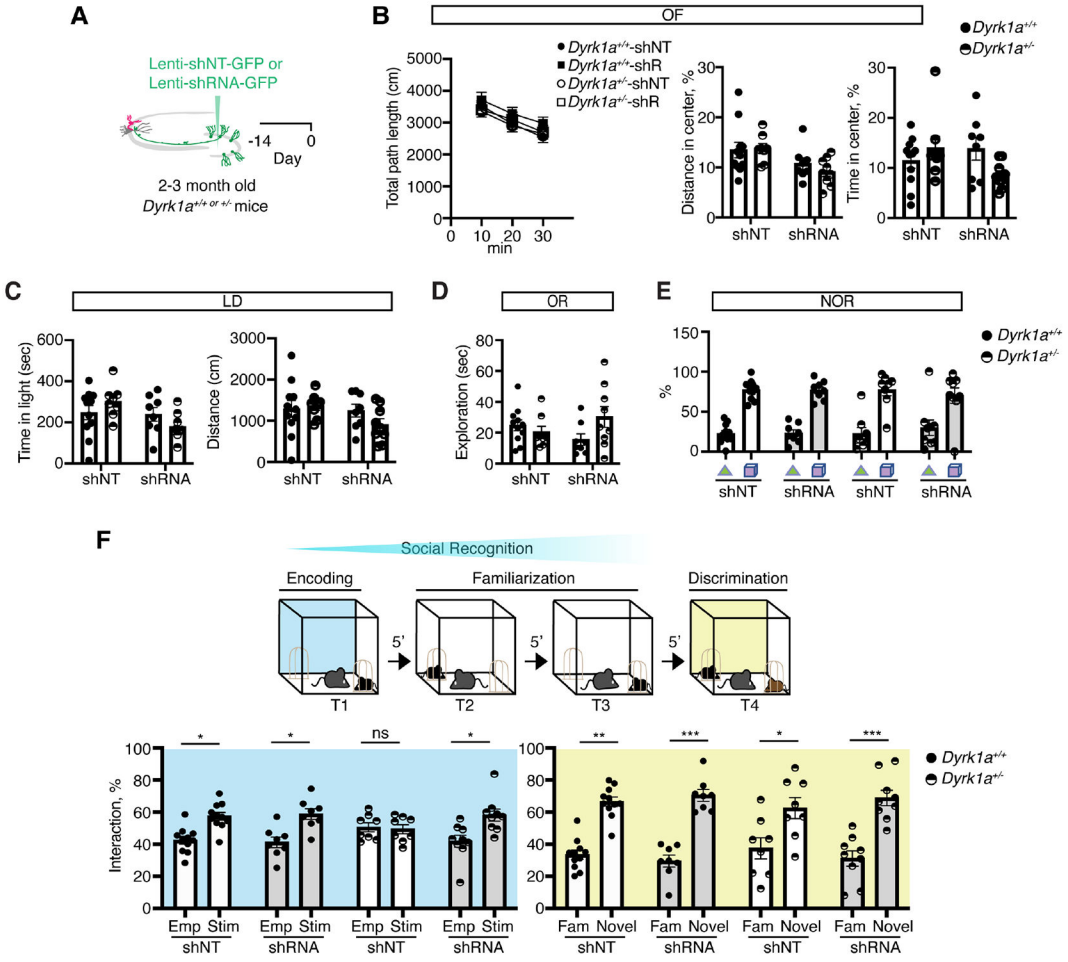

Figure 6. *Ablim3* downregulation in DGCs of adult heterozygous *Dyrk1a* mice restores social recognition

(A) Lentiviruses expressing *Ablim3* shRNA-GFP or non-targeting shRNA (shNT-GFP) were injected into DG of 2-3 month old *Dyrk1a*$^{+/+\ or\ +/-}$ mice.

(B-F) Behavioral analysis of *Dyrk1a*$^{+/+}$ mice injected with shNT (N=11 mice) or shRNA (N=8 mice) and *Dyrk1a*$^{+/-}$ mice injected with shNT (N=8 mice) or shRNA (N=9 mice) (see Figure S1F for behavioral testing schedule).

(B) OF, open field, quantification of total distance travelled, percentage of distance traveled across the center arena, percentage time in center.

(C) LD, light-dark box assay, quantification of time spent in the light compartment (seconds).

(D) OR, object recognition, quantification of the time spent sniffing the object (seconds).

(E) NOR, novel object recognition, quantification of the time spent sniffing the familiar object (triangle) and novel object (cube).

(F) Quantification of cup vs. social stimulus interaction time during social recognition phase (T1) (left panel, blue shaded) and the discrimination trial (T4, right panel, yellow shaded) These experiments are performed in male mice.

*$p < 0.05$; **$p < 0.01$; ***$p < 0.001$ using two-way ANOVA with Bonferroni post hoc test. All data are displayed as mean ± SEM.

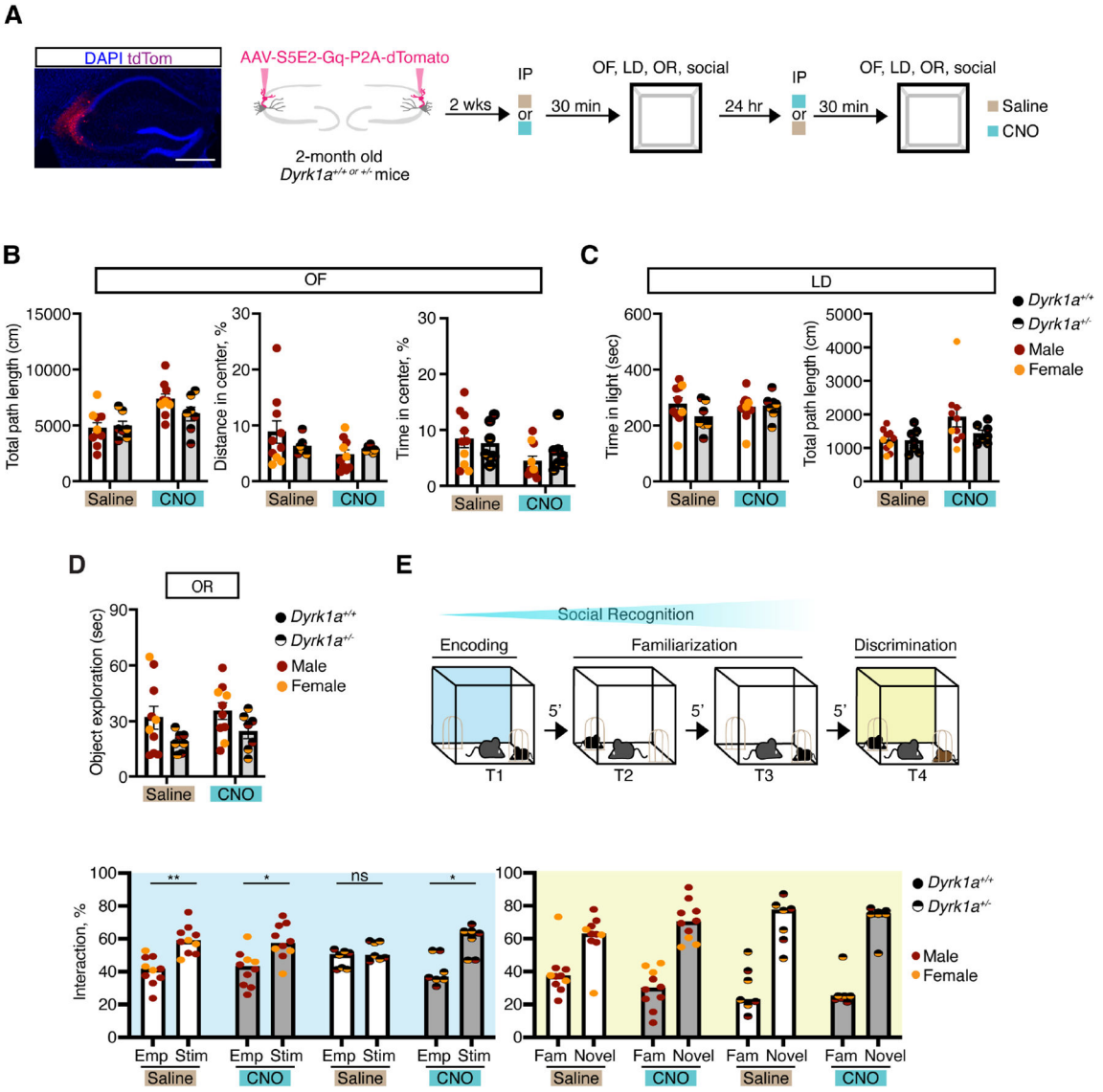

Figure 7. Acute chemogenetic activation of PV INs in CA3/CA2 of adult *Dyrk1a*$^{+/-}$ mice is sufficient to rescue social recognition

(A) Left, Representative image showing expression of hM3D(Gq)DREADD-tdTom in PV INs in CA3/CA2. Scale bar, 500 μm. Right, Schematic of chemogenetic activation of PV INs schedule. 2-month old *Dyrk1a*$^{+/+ \text{ or } +/-}$ mice were injected with AAV-S5E2-Gq virus into dCA2/CA3 2 weeks prior to behavioral testing using a vehicle/CNO cross-over design. Mice were injected with saline or 1mg/kg CNO 30 min prior to behavioral testing. 24 hours later mice were counterbalanced for vehicle/CNO and behaviorally tested.

(B-D) Chemogenetic activation of PV INs in CA3/CA2 of does not affect locomotion (OF) or anxiety-like (LD) behavior (B and C) and object recognition (D).

(E) Quantification of cup vs. social stimulus interaction time during social recognition phase (T1) (left panel, blue shaded) and the discrimination trial (T4, right panel, yellow shaded) (N= 10 mice for *Dyrk1a*$^{+/+}$ group; N= 7 mice for *Dyrk1a*$^{+/-}$ group).

These experiments are performed in male and female mice.

$^{*}p < 0.05$; $^{**}p < 0.01$; $^{***}p < 0.001$ using two-way ANOVA with Bonferroni post hoc test. All data are displayed as mean ± SEM.

See also Figure S8.

KEY RESOURCES TABLE

REAGENT or RESOURCE	SOURCE	IDENTIFIER
Antibodies		
Mouse anti-Ablim3 antibody, 1/100	Abcam	Ab67721; RRID: AB_1140118
Rabbit anti-Dyrk1a antibody, 1/100	Abnova	PAB31453
Mouse anti-PV antibody, 1/1000	Millipore	MAB1572; RRID: AB_2174013
Rabbit anti-PV antibody, 1/3000	Swant	PV25; RRID: AB_10000344
Goat anti-PV antibody, 1/5000	Swant	PVG213; RRID: AB_2721207
Guinea pig anti-vGlut1 antibody, 1/3000	Synaptic systems	135304; RRID: AB_887878
Rabbit anti-ZO1 antibody, 1/500	Invitrogen	402200; RRID: AB_431613
Goat anti-GFP antibody, 1/500	Novus	NB100-1770; RRID: AB_10128178
Rabbit anti-RFP antibody, 1/500	Rockland	600-401-379; RRID: AB_2209751
Mouse anti-RGS14 antibody, 1/400	NeuroMab	75-170; RRID: AB_2179931
Donkey anti-mouse-Alexa-488 antibody, 1/500	Jackson ImmunoResearch	715-545-150; RRID: AB_2340846
Donkey anti-rabbit-Alexa-Cy3 antibody, 1/500	Jackson ImmunoResearch	711-165-152; RRID: AB_2307443
Donkey anti-guinea pig-Alexa-647 antibody, 1/500	Jackson ImmunoResearch	706-605-148; RRID: AB_2340476
Donkey anti-goat-Alexa-488 antibody, 1/500	Jackson ImmunoResearch	705-545-003; RRID: AB_2340428
Donkey anti-sheep-Alexa-488 antibody, 1/500	Jackson ImmunoResearch	713-545-003; RRID: AB_2340744
Bacterial and virus strains		
Lentivirus-U6-shNT-Ubi-GFP	Sahay Lab	N/A
Lentivirus-U6-shRNA(*Ablim3*)-Ubi-GFP	Sahay Lab	N/A
AAV-S5E2-dTom-P2A-nlsdTom	Addgene	Addgene viral prep # 135630-PHPeB
AAV-S5E2-Gq-P2A-dTom	Addgene	Addgene viral prep # 135635-PHPeB
Lentivirus-CamKIIα-Cre-T2A-GFP	VectorBuilder	N/A
Lentivirus-U6-shNT-Ubi-Cre-T2A-GFP	Sahay Lab	N/A
Lentivirus-U6-shRNA(*Ablim3*)-Ubi-Cre-T2A-GFP	Sahay Lab	N/A
AAV-CamKIIα-hChR2(H134R)-eYFP	Addgene	Addgene viral prep # 26969-AAV5
Lentivirus-Ubi-GFP-IRES-***Ablim3***-*WT*	Sahay Lab	N/A
Lentivirus-Ubi-GFP-IRES-*Ablim3-SD*	Sahay Lab	N/A
Lentivirus-Ubi-GFP-IRES-*Ablim3-SA*	Sahay Lab	N/A
Chemicals		
Clozapins *N*-oxide	Tocris Bioscience	Cat #4936
DAPI Fluoromount-G®	Southern Biotech	Cat #0100-20
Biocytin	Sigma	Cat #B1758

REAGENT or RESOURCE	SOURCE	IDENTIFIER
Experimental models		
Dyrk1a^{tm1Jdc}/J	The Jackson Lab.	RRID: IMSR_JAX:027801
Tg(EIIa-cre)C5379Lmgd/J	The Jackson Lab.	RRID: IMSR_JAX:003724
Ai14(RCL-tdT)-D	The Jackson Lab.	RRID: IMSR_JAX:007914
Software and algorithms		
Image-J software	ImageJ	http://imagej.nih.gov/ij/
Prism 9	Graphpad	RRID:SCR_002798
EthoVision XT 15	Noldus	RRID:SCR_004074
EasyElectrophysiology software (V2.4.1)	EasyElectrophysiology	
Clampfit (V11.2)	Molecular Devices	